The Astrophysical Journal, 701:105–121, 2009 August 10 doi:10.1088/0004-637X/701/1/105

NTT, *SPITZER*, AND *CHANDRA* SPECTROSCOPY OF SDSSJ095209.56+214313.3: THE MOST LUMINOUS CORONAL-LINE SUPERNOVA EVER OBSERVED, OR A STELLAR TIDAL DISRUPTION EVENT?

S. Komossa[1], H. Zhou[1,6], A. Rau[2], M. Dopita[3], A. Gal-Yam[4], J. Greiner[1], J. Zuther[5], M. Salvato[2], D. Xu[7], H. Lu[1,6], R. Saxton[8], and M. Ajello[9,10]

[1] Max-Planck-Institut für extraterrestrische Physik, Postfach 1312, 85741 Garching, Germany; skomossa@mpe.mpg.de
[2] California Institute of Technology, 105-24 Robinson 1200 E. California Blvd., Pasadena, CA 91125, USA
[3] Research School of Astronomy and Astrophysics, The Australian National University, Cotter Road, Weston Creek, ACT 2611, Australia
[4] Benoziyo Center for Astrophysics, Weizmann Institute of Science, 76100 Rehovot, Israel
[5] I. Physikalisches Institut, Universität zu Köln, Zülpicher Str. 77, 50937 Köln, Germany
[6] Center for Astrophysics, University of Science and Technology of China, Hefei, Anhui, 230026, China
[7] National Astronomical Observatories, Chinese Academy of Science, A20 Datun Road, Chaoyang District, Beijing 100012, China
[8] ESA/ESAC, Apartado 78, 28691 Villanueva de la Canada, Madrid, Spain
[9] SLAC National Accelerator Laboratory, 2575 Sand Hill Road, Menlo Park, CA 94025, USA
[10] KIPAC, 2575 Sand Hill Road, Menlo Park, CA 94025, USA
Received 2009 February 17; accepted 2009 June 10; published 2009 July 20

ABSTRACT

The galaxy SDSSJ095209.56+214313.3 (SDSSJ0952+2143 hereafter) showed remarkable emission-line and continuum properties and strong emission-line variability first reported in 2008 (Paper I). The spectral properties and low-energy variability are the consequence of a powerful high-energy flare which was itself not observed directly. Here we report follow-up optical, near-infrared (NIR), mid-infrared (MIR), and X-ray observations of SDSSJ0952+2143. We discuss outburst scenarios in terms of stellar tidal disruption by a supermassive black hole, peculiar variability of an active galactic nucleus (AGN), and a supernova (SN) explosion, and possible links between these scenarios and mechanisms. The optical spectrum of SDSSJ0952+2143 exhibits several peculiarities: an exceptionally high ratio of [Fe VII] transitions over [O III], a dramatic decrease by a factor of 10 of the highest-ionization coronal lines, a very unusual and variable Balmer line profile including a triple-peaked narrow component with two unresolved horns, and a large Balmer decrement. The MIR emission measured with the *Spitzer* IRS in the narrow 10–20 μm band is extraordinarily luminous and amounts to $L_{10-20\,\mu\mathrm{m}} = 3.5 \times 10^{43}$ erg s^{-1}. The IRS spectrum shows a bump around $\sim$11 μm and an increase toward longer wavelengths, reminiscent of silicate emission. The strong MIR excess over the NIR implies the dominance of relatively cold dust. The pre- and post-flare NIR host galaxy colors indicate a nonactive galaxy. The X-ray luminosity of $L_{\mathrm{x},0.1-10\,\mathrm{keV}} = 10^{41}$ erg s^{-1} measured with *Chandra* is below that typically observed in AGNs. Similarities of SDSSJ0952+2143 with some extreme SNe suggest the explosion of a SN of Type IIn. However, an extreme accretion event in a low-luminosity AGN or inactive galaxy, especially stellar tidal disruption, remain possibilities, which could potentially produce a very similar emission-line response. If indeed a SN, SDSSJ0952+2143 is one of the most distant X-ray- and MIR-detected SNe known so far, the most MIR luminous, and one of the most X-ray luminous. It is also by far the most luminous ($> 10^{40}$ erg s^{-1}) in high-ionization coronal lines, exceeding previous SNe by at least a factor of 100.

Key words: circumstellar matter – galaxies: general – galaxies: individual (SDSSJ095209.56+214313.3) – supernovae: general

1. INTRODUCTION

Transient phenomena have been detected in various astrophysical object classes. They are especially pronounced in the high-energy regime, and provide us with important information on the physics of astrophysical sources under extreme conditions. Many of the transient phenomena are linked, in one way or another, to the presence of compact objects and especially black holes and the physical processes in their immediate environment. Transience in the high-energy domain covers a broad range of timescales ranging from typically milliseconds–seconds in gamma-ray bursts (GRBs; Klebesadel et al. 1973; Piran 2005), over minutes–hours in X-ray bursts (Grindlay et al. 1976; Lamb 2000) and early stages of supernova (SN) explosions (Soderberg et al. 2008), to weeks–months in stellar tidal disruptions (Rees 1988; Komossa & Bade 1999), for instance. Other transient events have been predicted by theory, but not yet observed, including long-lasting accretion disk flares of recoiling supermassive black holes (SMBHs; Shields & Bonning 2008), or very short-timescale hard X-ray flares due to tidal detonations of stars (Brassart & Luminet 2008).

Powerful outbursts of radiation do not only carry key information about their production mechanisms, they also can be used as a probe of their gaseous environment: the radiation is reprocessed into ultraviolet (UV), optical, infrared (IR), and X-ray emission lines which contain a wealth of information on the gaseous kinematics, chemical composition, density, and geometry of the line-emitting gas. In the context of SN explosions, reprocessing of high-energy radiation into emission lines carries information on the progenitor star and the circumstellar medium (CSM; Chugai & Danziger 1994; Filippenko 1997). Accretion flares from stars tidally disrupted by massive black holes will illuminate the stellar post-disruption debris and the interstellar medium (ISM), potentially including broad- and narrow-line regions and molecular tori at the cores of galaxies.

We have found SDSSJ0952+2143 (Komossa et al. 2008) at redshift $z = 0.079$ in a systematic search for emission-line galaxies in SDSS-DR6 (Sloan Digital Sky Survey Data

Table 1
Sequence of Events & Observations

Date	Type of Observation[a]	Waveband or Filter	Comments and Source Brightness
1990 Nov	RASS	0.1–2.4 keV	No X-ray detection
			$f_X < 5 \times 10^{-13}$ erg cm^{-2} s^{-1} (unabsorbed flux, 0.2–2 keV)
1993 Dec	NVSS	1.4 GHz	No radio detection
			$f_R < 1$ mJy
1998 Jan 23	2MASS	J,H,K_s	IR detection of extended emission; likely pre-flare state
			J = 15.4, H = 14.5, K_s = 14.4 mag
2002 May 7	*XMM-Newton* slew	0.2–10 keV	No X-ray detection
			$f_X < 5.5 \times 10^{-12}$ erg cm^{-2} s^{-1} (unabsorbed flux, 0.2–10 keV)
2004 Dec 20	SDSS photometry	u,g,r,i,z	Peculiar SED and i,z high-point, highest observed state
			u = 18.34, g = 17.7, r = 17.11, i = 16.65, z = 16.22 mag (SDSS DR7)
2005 Mar –	*Swift* BAT survey	15–55 keV	No X-ray detection
2008 Mar			$f_X < 8 \times 10^{-12}$ erg cm^{-2} s^{-1} (unabsorbed flux, 15–55 keV)
2005 Dec 30	SDSS spectroscopy	3900–9100 Å	Strong emission lines incl. iron; continuum fainter than during photometry
2006 Mar 02	*GALEX*	NUV, FUV	Blue color
			NUV = 20.2 mag, FUV = 19.9 mag
2007 Dec			Source noticed by us, searching the SDSS data base
2007 Dec 4–15	Xinglong spectroscopy	4000–8000 Å	Highest-ionization iron lines, He II, and broad Hα decreased in strength
2008 Jan 1	GROND photometry	g,r,i,z,J,H,K_s	Confirms the galaxy (core) got fainter in the optical band
2008 Feb 4	*Chandra*	0.1–10 keV	First detection of faint X-ray emission; implies high amplitude of variability
			$f_X \simeq 6.3 \times 10^{-15}$ erg cm^{-2} s^{-1} (unabsorbed flux, 0.1–10 keV)
2008 Feb 6	NTT spectroscopy	3800–8600 Å	Confirms fading lines in broader wavelength range
2008 Apr & May	*Triple Spec* spectroscopy	NIR	NIR emission lines detected; analysis ongoing
2008 Jun 5	*Spitzer* IRS	9.9–19.6 μm	Search for emission lines; first MIR SED measurement
			$f_{IR} = 12$ mJy at 12.5 μm
2008 Dec 25	Xinglong spectroscopy	4000–8000 Å	Some iron lines fainter
2009	*Chandra*	0.1–10 keV	X-ray monitoring; to be carried out

Note.[a] The following abbreviations have been used: RASS (*ROSAT* all-sky survey; Voges et al. 1999); NVSS (NRAO VLA Sky Survey; Condon et al. 1998); 2MASS (Two Micron All Sky Survey; Skrutskie et al. 2006); *GALEX* (*Galaxy Evolution Explorer*; Martin et al. 2005), GROND (Gamma-Ray Burst Optical/NIR Detector, Greiner et al. 2008); and NTT (New Technology Telescope).

Release 6; Adelman-McCarthy et al. 2008). The optical spectrum of SDSSJ0952+2143 and its multiwavelength properties turned out to be exceptional. The optical spectrum is dominated by strong iron coronal lines with the highest ratios of several [Fe VII] transitions over [O III]5007 measured among galaxies. The Hα profile shows a multipeaked structure. The highest-ionization iron lines have significantly faded between 2005 and 2007, and the optical continuum emission has decreased. These properties were interpreted as an emission-line and continuum response to a powerful high-energy flare (Komossa et al. 2008; hereafter Paper I) which itself escaped detection. After the initial recognition of the unusual spectrum and quick optical follow-up spectroscopy in 2007 December, we have initiated a number of multiwavelength observations, especially having in mind the possibility of using the emission-line response to the flare as a rare chance to do reverberation mapping of the different systems of gaseous matter in the galaxy core. Here, we report follow-up spectroscopy in the IR, optical, and X-ray band, and explore outburst scenarios. The paper is structured as follows: in Section 2 we present the new optical, IR, and X-ray observations and describe the data analysis. In Section 3, we use emission-line and continuum properties as diagnostics of the physical conditions in the line-emitting gas. Section 4 scrutinizes scenarios which could explain the unusual multiwavelength properties of SDSSJ0952+2143, with focus on a SN explosion, exceptional active galactic nucleus (AGN)-type variability, and tidal-disruption-related scenarios. The conclusions are provided in Section 5. In Table 1 an overview of the previous and new observations and the sequence of events is presented. We use a cosmology (Wright 2006) with $H_0 = 70$ km s^{-1} Mpc^{-1}, $\Omega_M = 0.3$, and $\Omega_\Lambda = 0.7$ throughout this paper.

2. MULTIWAVELENGTH OBSERVATIONS

2.1. New Technology Telescope Optical Spectroscopy

2.1.1. Data Reduction

We have observed SDSSJ0952+2143 with EMMI[11] at the ESO-New Technology Telescope (NTT) 3.5 m telescope on 2008 February 8 (hereafter referred to as 2008 NTT spectrum). We took two exposures each of 1500 s duration with grism #5 (wavelength range: 3800 Å–7000 Å) and #6 (wavelength range: 5800 Å–8600 Å), respectively, using a slit width of 1.5 arcsec oriented at the parallactic angle (Filippenko 1982). This setting gave a spectral resolution of ∼6 Å. KPNO standard stars were observed before and after each target exposure for flux calibration. He–Ne–Ar lamp spectra were obtained with the two grisms in order to carry out the wavelength calibration.

The raw two-dimensional data were reduced with standard procedures using the software package IRAF.[12] The CCD data reduction includes bias subtraction, flat-field correction, and cosmic-ray removal. The task *apall* was used to extract the spectra. We then carried out the wavelength and flux calibration using the He–Ne–Ar lamp spectra and the standard stars. After flux calibration the two spectra obtained with grism#5 agree within 4% with each other, and with one of the two grism#6 spectra within 8%. The second grism#6 exposure deviated in its normalization which could be traced back to a change in seeing

[11] See the EMMI user's manual at http://www.ls.eso.org/docs/LSO-MAN-ESO-40100-0001/LSO-MAN-ESO-40100-0001.pdf.
[12] IRAF is distributed by the National Optical Astronomy Observatories, which is operated by the Association of Universities for Research in Astronomy, Inc., under cooperative agreement with the National Science Foundation.

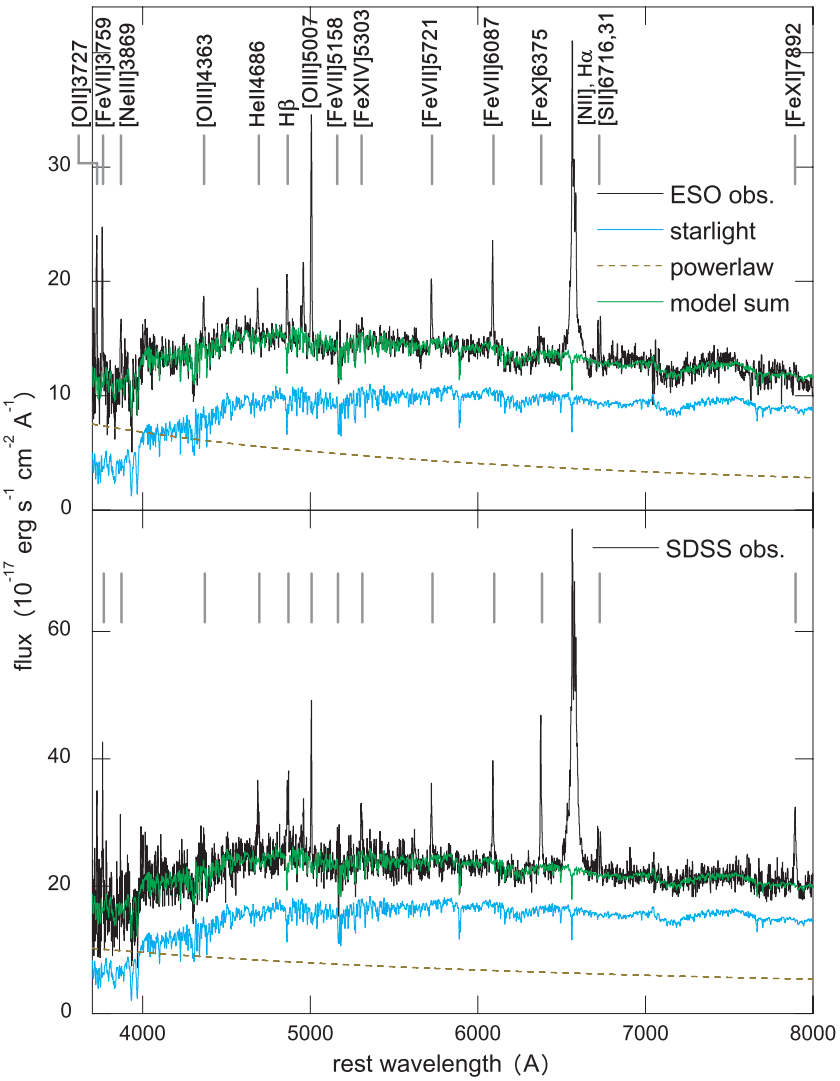

Figure 1. 2005 SDSS spectrum (lower panel) and the 2008 ESO NTT spectrum (upper panel) of SDSSJ0952+2143. Emission lines are labeled. The continuum emission was decomposed into stellar (blue solid line) and power-law (index $\alpha_\lambda = -1.2$ (SDSS) and -0.7 (NTT); light green dashed line) component as given in the graph.

during that target exposure, and this spectrum was therefore shifted in flux scale to match the other three spectra. The spectra were corrected for Galactic extinction of $E(B-V) = 0.028$. All four spectra were then combined and the resulting spectrum is shown in Figure 1 where it is compared with the previous SDSS spectrum which was taken in 2005. Telluric absorption was corrected for, using the standard stars and taking into account the air mass during the observations.

2.1.2. Underlying Spectral Energy Distribution

Using the flux calibration scheme described above, the observed continuum level, dominated by starlight from the host galaxy, is lower in the NTT spectrum than in the SDSS spectrum, which can be traced back to aperture loss due to the extended host galaxy. The flux in the [O III]5007 emission line is consistent with being constant between the 2005 SDSS and 2008 ESO NTT observation (Table 1). In any case, when using emission-line ratios for diagnostics, we preferentially use neighboring emission lines, to be more independent of residual absolute calibration uncertainties.

The SDSS and NTT spectra were decomposed into a stellar and a nonstellar (power-law) component using the method described by Lu et al. (2006; see also Zhou et al. 2006), and are both dominated by the stellar component of the host galaxy. The continuum emission from the host galaxy can be well fit with a single stellar population with an age of $T \simeq 2$ Gyr. The underlying nonstellar continuum component is very faint in the NTT spectrum. In Paper I, we used instead a mix of synthesized galaxy template spectra to describe the host galaxy emission, rather than one single stellar population. Re-modeling of the continuum introduces slight changes (typically $<$10%–20%) in the remeasured emission lines reported here.

2.1.3. Narrow Emission Lines

After the spectral energy distribution (SED) was decomposed into host galaxy and power-law contribution (Figure 1), these components were subtracted from the spectrum and the emission lines were then measured. Emission-line widths reported here and in Paper I have been corrected for instrumental broadening. Most emission lines which were present in the 2005 SDSS spectrum are still detected in the 2008 NTT spectrum, even though a number of them, especially the highest ionization lines, the broad Balmer lines, and the peculiar narrow Balmer horns, are significantly fainter (see below). We identify transitions of

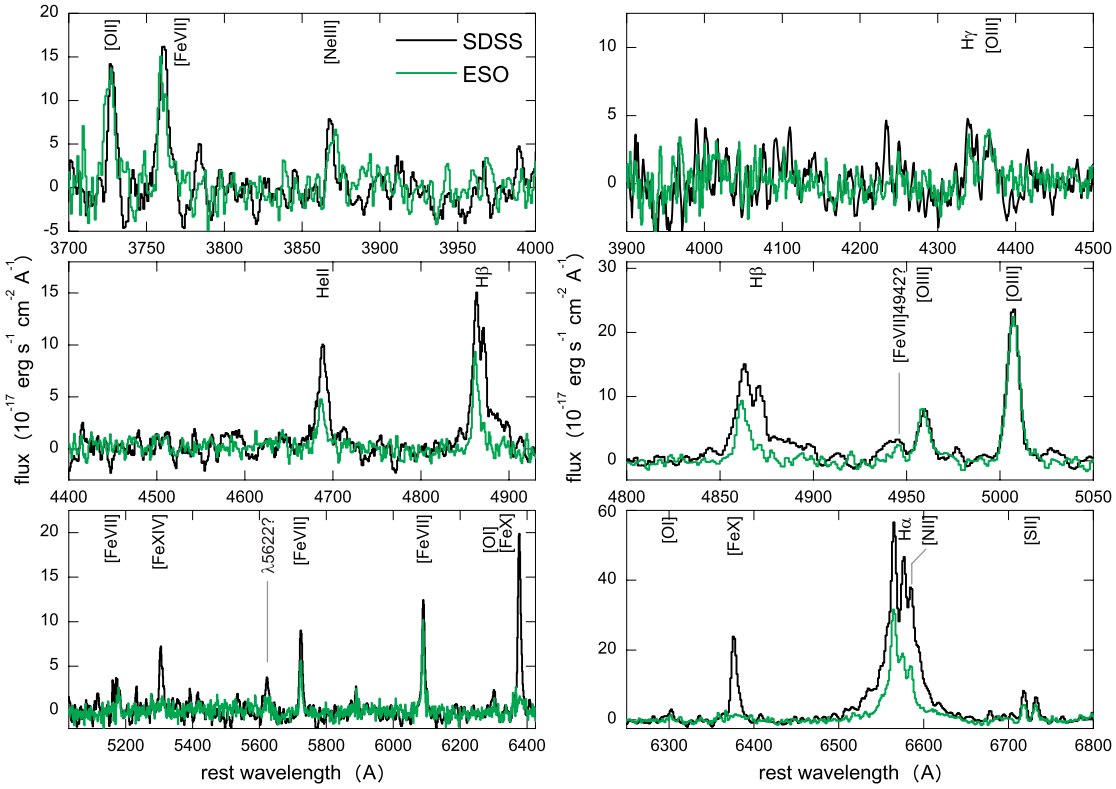

Figure 2. Zoom on individual emission-line complexes after continuum subtraction (note the different flux and wavelength scale in each panel, optimized to display emission lines of different strengths). SDSS (black) and ESO NTT (green) spectrum are overplotted on top of each other. The resolution of the SDSS spectrum was degraded to match that of the NTT spectrum. Prominent emission lines are marked.

[O I], [O II], [O III], [N II], [S II], He II, [Ne III], [Fe VI], Fe [VII], [Fe X], [Fe XI], [Fe XIV], and Balmer lines (Figures 1, 2, 3, and 4).

We have first refit all emission lines of the 2005 SDSS spectrum with a single Gaussian component, and then did the same for the 2008 NTT spectrum. Single Gaussian fits to those emission lines which do not show spectral complexity result in line widths of 200–300 km s^{-1} in the SDSS spectrum. These same lines are not resolved in the NTT spectrum, which was of lower resolution, consistent with constant line width. Most of the high-ionization lines appear broader than the low-ionization lines, indicative of a two-component nature of their line profiles (see below). FWHMs based on single Gaussian fits listed in Table 2 should therefore not be used per se, but should rather be taken as an indication of a more complex emission-line profile, if the line width exceeds ∼300 km s^{-1}.

As already noted in Paper I, the highest-ionization iron lines have strongly faded. Here we greatly improve limits on [Fe X] and [Fe XIV] and for the first time include [Fe XI] in the NTT spectral band, in comparison with the earlier 2007 Xinglong follow-up spectroscopy. [Fe XI] is a factor ∼10 fainter in the 2008 NTT spectrum than it was in the 2005 SDSS spectrum. [Fe X] is very faint, even though the exact measurement is hampered by uncertainties in the precise correction of the superposed telluric (atmospheric) absorption.

The line emission from [O III]4363 and HeII4686 is remarkably strong in the 2005 and 2008 spectra, with intensity ratios [O III]4363/[O III]5007 = 0.2, and HeII4686$_{totl}$/Hβ_n = 2 in 2005 (while HeII4686$_n$/Hβ_n = 0.3, below the value of 0.66 above which the ratio is dominated by helium abundance; Dopita & Sutherland 2003). Here, the index *totl* refers to the total line emission, while the index *n* refers to the emission of the narrow component. HeII4686$_{totl}$/Hβ_n decreased by a factor 2.8 which can be traced back to a decrease in the broad component in He II (Section 2.1.4).

We have compared the 2007 Xinglong spectrum (Paper I) with the 2008 NTT spectrum in order to search for spectral variations on the timescale of two months. Keeping in mind the lower S/N and resolution of the Xinglong spectrum, emission lines are consistent with being constant within better than a factor of 2. A new optical spectrum was acquired with the 2.16 m Xinglong telescope on 2008 December 25 with an exposure time of 7200 s. The strongest emission lines are still all present and no new spectral features have emerged. [Fe VII]5722 is no longer safely detected, indicating a decrease of this line at the 3σ level. The full results of this and future optical monitoring will be presented elsewhere.

2.1.4. Two-Component High-Ionization Lines

When fit by single Gaussians, several of the high-ionization lines show a relatively broad profile, and are in fact better modeled by two components; a broad base and a narrow core. Seven lines in the SDSS spectrum are strong enough for such a decomposition, while for only two of them the decomposition can still be done with the NTT spectrum. These seven lines are [Fe VII]3759, HeII4686, [O III]5007, [Fe VII]5722, [Fe VII]6087, [Fe X]6376 and [Fe XI]7894. If the narrow core of each line is fixed to the FWHM of [S II], 210 km s^{-1}, the broad base is well fit by a second Gaussian with a width of ∼600–800 km s^{-1} ([Fe VII]5722, [Fe X]6376, [Fe VII]3759 and [Fe XI]7894), 900–1100 km s^{-1} ([Fe VII]6087 and He II), and 400 km s^{-1} ([O III]5007), respectively. [Fe VII]6087 and HeII4686 can still be decomposed in the ESO spectrum and were represented by a two-component Gaussian assuming that

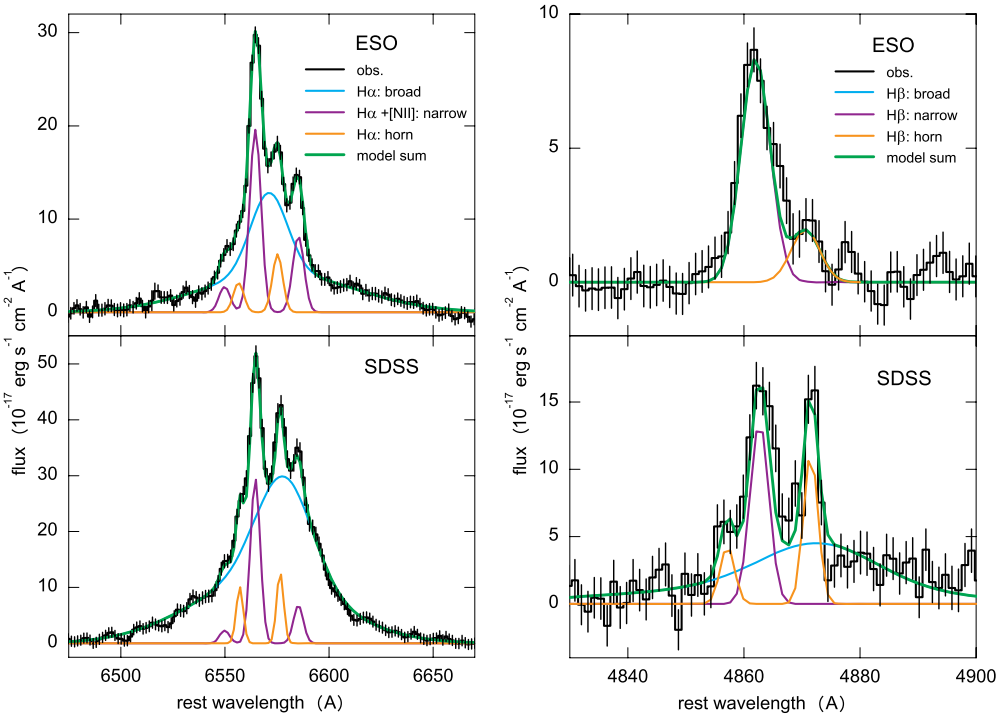

Figure 3. Decomposition of the Balmer-line profiles of Hα (left) and Hβ (right) into several components. The lower panel shows the 2005 SDSS data, the upper panel the 2008 ESO NTT data (note that the flux scale is different on each axis). The different components of the profile are labeled in each figure. Note the change in the broad component and the two narrow horns which are all fainter in the 2008 spectrum.

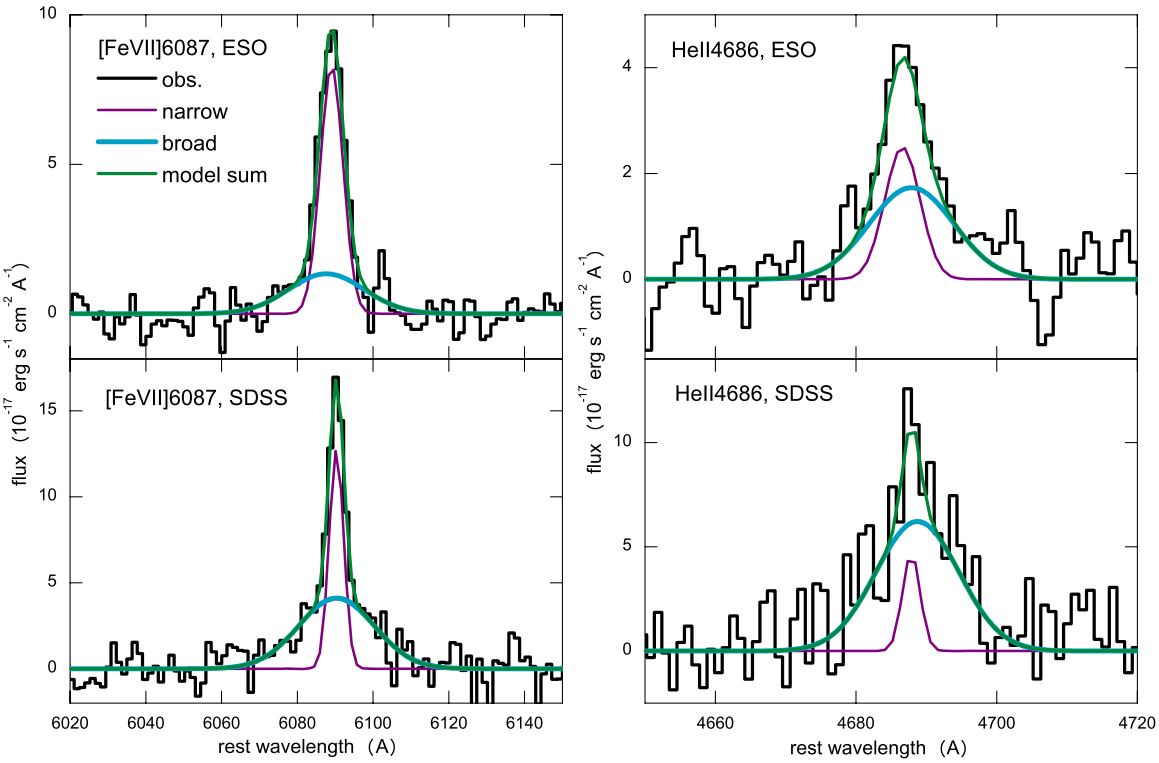

Figure 4. Decomposition of the two bright high-ionization lines He II4686 and [Fe VII]6087 into two components. The broad base which is present in the 2005 SDSS spectrum is much fainter in the 2008 ESO NTT spectrum.

neither the width of the broad component nor that of the narrow component varied between 2005 and 2008 (and taking into account the different instrumental broadening). We find that the flux in the narrow component is almost constant, while the broad component decreased by at least a factor of ∼3 (Figure 4).

2.1.5. Balmer Line Profile and Variability

We paid special attention to changes in the very unusual profile of the Balmer lines, which consist of several components: an asymmetric broad base, a narrow core, and two strong peculiar unresolved horns. We carefully decomposed the line

Table 2
Emission-Line Ratios Relative to [O III]5007, Measured in the 2005 SDSS Spectrum, and the 2008 NTT Spectrum

Line	λ	$I/I_{[O\,III]}$[a] SDSS	FWHM SDSS	$I/I_{[O\,III]}$ ESO NTT	Ratio[b] ESO/SDSS
[Fe VII]	3586	0.44	230	...	...
[O II]	3727	0.51	350	0.57	1.16
[Fe VII]	3759	0.74	515	0.47	0.67
[Ne III]	3869	0.22	150	0.25	1.18
Hγ	4340	0.24	380	0.13	0.57
[O III]	4363	0.23	710	0.27	1.20
He II	4686	0.72	820	0.25	0.36
$H\beta_n$	4861	0.33	210!	0.30	0.95
$H\beta_{horn,blue}$		0.09 :	Unresolved	< 0.03 :	< 0.39
$H\beta_{horn,red}$		0.23	Unresolved	0.07 :	0.32
$H\beta_b$		0.79	2100	< 0.58	< 0.76
[Fe VII]?	4942	0.22	690	0.10	0.47
[O III]	5007	1.0[a]	330	1.0	1.04
[Fe VII]	5158	0.14	300	< 0.03	< 0.25
[Fe VI]	5176	0.38	1180:	...	...
[Fe XIV][c]	5303	0.44	620	0.06 :	0.13
?	5621	0.35	820	0.08	0.24
[Fe VII]	5722	0.56	450	0.25	0.46
[Fe VII]	6087	0.67	320	0.50	0.76
[Fe X]	6375	1.17	370:	0.14 :	0.12
[O I]	6300	0.12	210!	0.05	0.41
$H\alpha_n$	6564	1.06	210!	0.78	0.77
$H\alpha_{horn,blue}$		0.32	Unresolved	0.06	0.2
$H\alpha_{horn,red}$		0.50	Unresolved	0.1	0.24
$H\alpha_b$		9.7	2100	3.29	0.35
[N II]	6584	0.25	2.0!	0.32	1.38
[S II]	6716	0.31	210	0.17	0.56
[S II]	6731	0.24	210	0.15	0.65
[Fe XI]	7892	0.87	440	0.10	0.12

Notes.
[a] Line ratios reported in this table are based on single Gaussian fits to the emission lines, except for the broad components of Hα and Hβ which were represented by two Gaussians (see the text for details). For each epoch, line ratios have been normalized to [O III]λ5007. The observed [O III] flux is $f_{[O\,III],SDSS} = 1.8 \times 10^{-15}$ erg cm^{-2} s^{-1} and $f_{[O\,III],ESO} = 1.9 \times 10^{-15}$ erg cm^{-2} s^{-1}, in the 2005 SDSS and 2008 NTT spectrum, respectively.
[b] The ratio is the direct flux ratio between 2005 SDSS and 2008 NTT emission lines.
[c] Potentially blended with [Ca V]5309 in the ESO spectrum. Line ratios marked with a colon are uncertain measurements, and an exclamation mark indicates that this parameter was fixed in the fitting procedure. A question mark indicates an uncertain line identification.

profiles, and searched for changes between the 2008 NTT spectrum and the 2005 SDSS spectrum. The Hα+[N II] blend in the SDSS spectrum was fit with seven Gaussians. (1) Three Gaussians for the "normal" narrow emission lines in Hα and [N II]6548,6584. The redshift and line widths were fixed to that of the [S II]6716,6731 doublet, and the [N II]6548/6584 ratio was fixed to the theoretical value of 1/3. (2) Two Gaussians for the narrow horns, with line width fixed to the instrumental resolution, and centroids and intensities as free parameters.[13] (3) Two Gaussians for the broad component of Hα with centroids, widths, and intensities as free parameters. Since the broad base is much broader than the narrow components and since the narrow horns are red- and blueshifted and do not coincide with the narrow core of Hα, the broad and narrow components can be relatively well decomposed. Errors in FWHM are typically less than 20%. At the same time, the two Gaussian components which make up the broad base of Hα are not well constrained individually. We therefore only report the FWHM of the sum of the two Gaussians that fit this component, and only report the total line flux, but no results on the two components separately.

The Hβ regime was fit with five Gaussians that match the components in Hα. (1) One Gaussian for the normal narrow Hβ emission line, with its centroid redshift and width fixed to that of the corresponding Hα line. (2) Two Gaussians for the narrow horns, also with their centroids and widths fixed to that of Hα. (3) Two Gaussians for the broad component of Hβ, with their centroids, widths, and the intensity ratio of the two Gaussians fixed to that of the broad component of Hα. The results of the decomposition are shown in Figure 3.

The Hα and Hβ complexes in the 2008 NTT spectrum were fit using the same scheme as for the 2005 SDSS spectrum, but all the widths of the narrow lines (including the narrow horns) which are unresolved, were fixed to the instrumental broadening. The two Gaussians for the broad component were not fixed to the SDSS values, and indeed both the intensity and profile of Hα changed significantly between the two observations, with an intensity ratio of 0.35 between the ESO and SDSS observation. The broad Hα component is still asymmetric with excess emission in the red part of the line with a centroid shift relative to the narrow core of $v_{SDSS} \simeq 560$ km s^{-1} (SDSS spectrum) in comparison to $v_{NTT} \simeq 270$ km s^{-1} (NTT spectrum), while the line width changed from FWHM $\simeq 2100$ km s^{-1} (SDSS) to FWHM $\simeq 1500$ km s^{-1} (NTT). The broad component in Hβ is no longer safely detected in the NTT spectrum.

The remarkable narrow horns remained fixed in red/blueshift (at $v = 540$ and -340 km s^{-1}, where a negative sign indicates blueshift), but got fainter (Table 2).

Hγ is too faint for any decomposition, and we merely report results from a single Gaussian fit in Table 2.

2.2. GROND JHK Photometry

Photometry was performed with the seven-channel imager GROND (Greiner et al. 2008) attached to the 2.2 m telescope at La Silla in the filters g, r, i, z and J, H, and K_s. The observations were carried out on 2008 January 1, at a seeing of 1″. Each observation consisted of four exposures with 46 s each in the visual and 24 exposures with 10 s each in the NIR channels, giving an effective exposure time of 4 minutes in the NIR and 3 minutes in the visual. The images were flatfield and bias corrected using standard IRAF routines. While the images in the visual bands are simply stacked after astrometric registration, the NIR images are first distortion corrected and then co-added with the shift-and-add method of the jitter command in the eclipse package (Devillard 1997).

Results from g, r, i, and z were reported in Paper I which showed that the luminosity of the galaxy core decreased by a factor 1.5–2 between the 2004 SDSS and the 2008 GROND photometry. Here we add the NIR results. The J, H, and K_s photometry was calibrated against the Two Micron All Sky Survey (2MASS) measurement of 1998. Given the different spatial resolutions of GROND and 2MASS, only the integrated emission can be compared. The total J, H, and K_s entries listed in the 2MASS catalogue of extended objects and cited in NED (Skrutskie et al. 2006) are J, H, K_s = (15.4,14.5,14.4) mag (see also Figure 5). We have selected sources in the field of view which have comparable brightness as SDSSJ0952+2143,

[13] In what follows we will generally assume that only these two strong horns are present, but note here that we cannot exclude the presence of more such components at very faint emission levels.

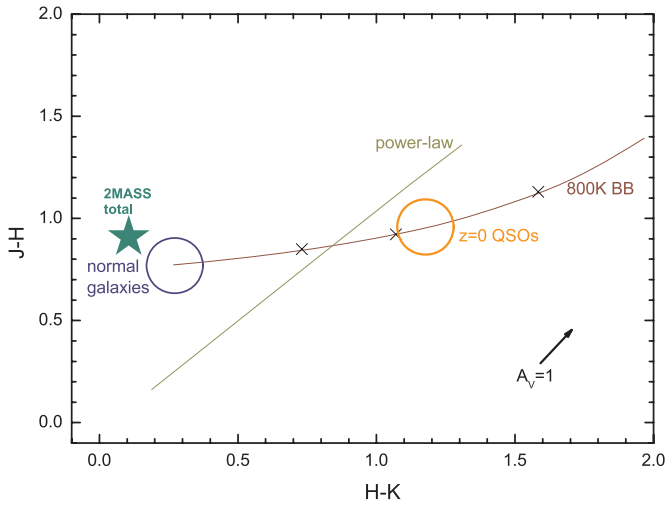

Figure 5. Locus of the 2MASS NIR colors of SDSSJ0952+2143 in comparison to the loci of quiescent galaxies and low-redshift QSOs (Hyland & Allen 1982). For comparison, the two curves represent a mix of a normal stellar population and a power-law or blackbody (800 K) emission component with increasing strength from left to right. The contribution of the stellar population decreases from left to right along the blackbody curve. Reddening by $A_V = 1$ is indicated by the arrow. The 2MASS data point lies in a region where normal galaxies are found.

(A color version of this figure is available in the online journal.)

and have used these to perform the GROND photometry. Given the faintness of the galaxy in the 2MASS exposure, we conservatively assign a photometric error of 0.5 mag. Within this error, the GROND magnitudes are consistent with 2MASS.

The J (H) coordinates of the galaxy center (J2000), R.A. = 09:52:09.54 (09:52:09.56) and decl. = +21:43:13.2 (+21:43:13.3), are consistent with the SDSS position. Radial profiles of the host galaxy of SDSSJ0952+2143 in comparison with the point-spread function of nearby stars show that the emission from the galaxy can be traced out to a radius of 3″–4″ in the J band. Close inspection of the J, H, K_s images reveals the emergence of a spiral structure at faint emission levels in all three images (Figure 6). Finally, we note that no other bright NIR source within a few arcseconds of SDSSJ0952+2143, which could have affected the 2MASS measurements, is detected (Figure 6).

2.3. Chandra, XMM-Newton, and ROSAT X-ray Observations

SDSSJ0952+2143 was observed and not detected during the *ROSAT* all-sky survey in November 1990. The upper limit on its PSPC count rate, <0.036 counts s^{-1}, translates into an upper limit on its (0.1–2.4) keV X-ray luminosity of $L_x < 10^{43}$ erg s^{-1} (assuming an X-ray power-law with photon index $\Gamma_x = -1.9$ and no excess absorption above the Galactic value, $N_{H,gal} = 2.79 \times 10^{20}$ cm^{-2}).

The field of SDSSJ0952+2143 was also covered during an *XMM-Newton* slew observation, slew 9044100004, on 2002 May 7. No photons from the source were detected, with an EPIC pn upper limit of 1.3 counts s^{-1}. Again assuming a spectrum with $\Gamma_x = -1.9$ and $N_{H,gal}$ gives an upper limit on the (0.2–10 keV) X-ray luminosity of $L_x < 8 \times 10^{43}$ erg s^{-1}.

SDSSJ0952+2143 was also not detected in X-rays during the *Swift* BAT survey (Markwardt et al. 2005; Ajello et al. 2008). The upper limit from three years of BAT survey observations between 2005 March and 2008 March is $f_x < 8 \times 10^{-12}$ erg cm^{-2} s^{-1} in the 15–55 keV band, or $L_x < 1 \times 10^{44}$ erg s^{-1} in the same band.

After the Xinglong and GROND detection of variability, we initiated a *Chandra* DDT observation (Paper I; ObsId 9814) which was carried out quasi-simultaneous with the NTT observation (Table 1). Had the source still been sufficiently bright in X-rays, this would have provided a unique chance to "reverberation-map" responses of the high-ionization lines to changes in the ionizing continuum. During the 10 ks ACIS-S observation, only faint X-ray emission was detected with a count rate of 7×10^{-4} counts s^{-1}. Among the detected photons, ~40% were above 3 keV, indicating a relatively hard X-ray spectrum, which is not strongly absorbed. Since the source is too faint to perform spectral fitting, we have used two characteristic models in order to estimate fluxes and luminosities. Assuming a spectrum with $\Gamma_x = -1.9$ and $N_{H,gal}$ gives an X-ray luminosity of $L_x = 4 \times 10^{40}$ erg s^{-1} (2–10 keV) and $L_x = 1 \times 10^{41}$ erg s^{-1} (0.1–10 keV). Using instead a thermal bremsstrahlung model with $kT = 10$ keV gives a similar (0.1–10 keV) luminosity of $L_x = 1 \times 10^{41}$ erg s^{-1}. The *Chandra* X-ray source is located at R.A. = 09:52:09.56, decl. = 21:43:13.3 (J2000) and agrees well with the SDSS coordinates, and with the GROND position. The astrometric accuracy of *Chandra* of 1″ corresponds to a projected scale of 1.5 kpc within the host galaxy.

2.4. Spitzer IR Observations

In order to search for emission lines excited by the flare, we initiated a DDT observation of SDSSJ0952+2143 with the *Spitzer Space Telescope*, which was carried out on 2008 June 5. The data also allow us to measure the IR SED, get clues on the type of host galaxy, and measure the post-flare IR luminosity, in comparison with previous measurements which indicated possible NIR variability (Paper I). For few, if any, of such extreme transients as SDSSJ0952+2143, MIR spectroscopy was ever done.

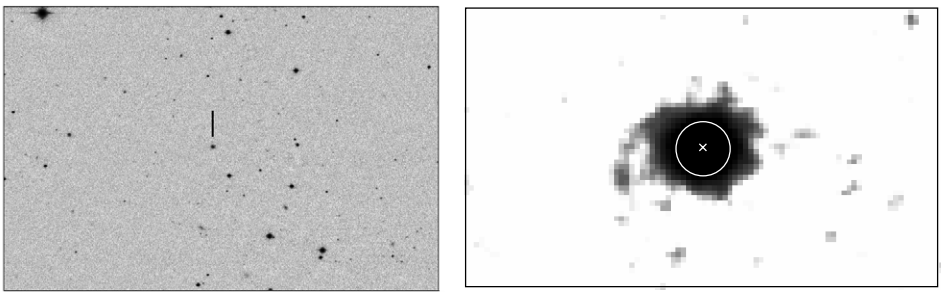

Figure 6. Left: GROND J-band image of the field of SDSSJ0952+2143 which is marked with the black bar. Right: zoom on the K_s-band image of SDSSJ0952+2143 and overlay of the *Chandra* X-ray position (white cross) plus error circle of 1″ radius.

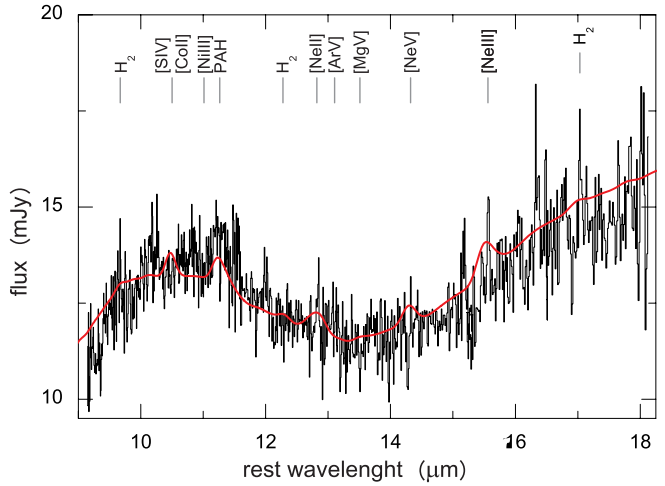

Figure 7. *Spitzer* SH IRS spectrum of SDSSJ0952+2143 taken in 2008 June. The broad bump around 11 μm and the increase toward longer wavelengths are reminiscent of dust emission from silicates. The red line overplots the *Spitzer* mean quasar SED of Netzer et al. (2007) which represents the shape of the overall spectrum well (its normalization was chosen such that it matches the flux of SDSSJ0952+2143 at 14 μm). The wavelengths of several emission lines typically observed in starburst galaxies, AGNs, and SNe are marked.

(A color version of this figure is available in the online journal.)

The observation was carried out with the Short-High module (SH; wavelength range 9.9–19.6 μm) of the InfraRed Spectrograph (IRS; Houck et al. 2004). We used the standard staring mode, in which the target is placed at two nod positions within the slit. Ten spectra with 120 s duration each were taken at each nod position, amounting to a total on-source exposure time of 2438 s. An off-source position was observed in a similar way to provide a measure of the background.

The raw data were processed by the *Spitzer* pipeline version 18.0.2 and the residual sky was subtracted from the resulting two-dimensional spectrum using the off-source observation. Bad pixels were removed and the areas then Poisson smoothed. Subsequently, one-dimensional spectra for each nod position were extracted from the Basic Calibrated Data with SPICE 2.1.2.[14] The spectra from the two nods were co-added and the final spectrum is shown in Figure 7.

SDSSJ0952+2143 was detected with a flux density of 12 ± 1 mJy at 12.5 μm. The global SED indicates excess emission around 11 μm, and an increase at longer wavelengths, and closely resembles the mean PG quasar *Spitzer* IRS SED of Netzer et al. (2007; their Figure 3). We have approximated the MIR SED by two black bodies (with $T_1 = 460$ K; the lower temperature of the second component is not well constrained). While this approximation is certainly too simple, we use this parameterization for an estimate of the luminosity. Integration over the narrow IRS SH band gives $L_{10-20\,\mu\mathrm{m}} = 3.5 \times 10^{43}$ erg s^{-1}, which is a safe lower limit on the total IR luminosity. Integrating over the higher-temperature blackbody component gives $L_{\mathrm{MIR}} = 9 \times 10^{43}$ erg s^{-1}.

We have searched for emission lines in the spectrum. These lines could either be excited by the flare, or else represent permanent emission from the host galaxy. As a guideline, we have paid attention to emission features which are commonly detected in the spectra of starburst galaxies, AGN, and SNe. Strong MIR lines frequently seen in AGN include [S IV]10.51 μm, [Ne II]12.81 μm, [Ne V]14.32 μm and [Ne III]15.56 μm, while occasionally [Ar V]13.10 μm, [Mg V]13.52 μm, and [Fe II]17.94 μm have been detected (e.g., Sturm et al. 2002; Netzer et al. 2007; Tommasin et al. 2008; Dale et al. 2009). The polycyclic aromatic hydrocarbon (PAH; Puget & Leger 1989) feature at 11.25 μm is frequently present, too, together with some molecular hydrogen lines. In SNe, transitions from Co and Ni have been detected (e.g., Roche et al. 1989; Kotak et al. 2006).

The relatively faint spectrum complicates the line searches. The enhanced fluctuations in the red part of the spectrum we trace back to noise. There is some evidence for the PAH feature at 11.25 μm, and emission lines of [Ne II]12.81 μm and [Ne III]15.56 μm. In order to assess the reality of the neon lines, we have extracted spectra from each nod position separately. There is evidence for these lines in both spectra. Other apparent features that appear in the spectrum coincide with regions of enhanced background noise. No strong emission from [Ne V]14.32 μm is detected. A more rigorous search for faint features is deferred to a future publication. Here, we conservatively use the measured flux in [Ne III] as upper limit for any true line emission, which gives $L_{[\mathrm{Ne\,III}]} < 2 \times 10^{40}$ erg s^{-1}.

3. EMISSION-LINE AND CONTINUUM DIAGNOSTICS

We now derive constraints on the physical conditions in the reprocessing material, which are later used in discussing outburst scenarios.

3.1. Forbidden Lines

Generally speaking, the wide range of ionization states we see, and the very different critical densities of transitions among the narrow forbidden lines (e.g., [S II], [O I] and up to [Fe XIV]), imply a wide range of densities in gas which is kinematically relatively quiescent with FWHMs of $\sim$ 200–800 km s^{-1}.

3.2. Multipeaked Balmer-Line Profile

The Balmer-line profile is complex, and variable in time. It consists of several kinematical components. (1) A broad component with a redshifted peak. The profile slightly narrowed and the peak shift slightly changed between 2005 and 2008. (2) A narrow component with a width similar to other forbidden lines, consistent with being constant between 2005 and 2008. (3) Two peculiar narrow, unresolved, horns, which are present in Hα and Hβ and which faded significantly between 2005 and 2008. We comment on each component in turn.

Broad component, Balmer decrement. As already remarked in Paper I, the Balmer decrement is very large, indicating either optical depth effects or a dominant contribution from collisional excitation (heavy extinction is unlikely, since correction for it would boost the already high Balmer-line luminosity even further). The intensity ratio Hα_{b}/Hβ_{b} changes from $\sim$ 12.2 to $>$ 5.7 between 2005 and 2008; Hβ_{b} is no longer safely detected in the 2008 NTT spectrum. The Hα luminosity during the 2005 SDSS observation is very large: $L_{\mathrm{H}\alpha_{\mathrm{b}}} = 3 \times 10^{41}$ erg s^{-1}. It decreased by a factor 3 between 2005 and 2008. Assuming an average luminosity of 2×10^{41} erg s^{-1} lasting for at least three years translates into an energy of at least 2×10^{49} erg in Hα only. While the broad Hα component may well be completely dominated by collisional excitation, the narrow components of Hα and [O III] are still almost as luminous ($L_{\mathrm{H}\alpha_{\mathrm{n}}} = 2.5 \times 10^{40}$ erg s^{-1}) in 2008 as the detected X-ray emission. This either implies that the continuum source is partly obscured while the Balmer-line emitting region is not, or there

[14] http://ssc.spitzer.caltech.edu/postbcd/spice.html

is a strong EUV contribution to the SED, or we see time delay effects of a once brighter continuum. The broad Hα component is redshifted by ~600 km s^{-1} in 2005 (Paper I), and still by 300 km s^{-1} in 2008. This redshift likely reflects a true kinematic shift. If it was due to extinction or optical depth effects in a shell geometry, the receding, more distant, red part of the line would be more affected (which would cause an apparent blueshift of the centroid).

Narrow component. This component has similar width than other narrow lines. The Balmer decrement, $H\alpha_n/H\beta_n = 3.2$ (2005) and 2.6 (2008) is close to the Case B recombination value, indicating little global extinction along the sightline within the host galaxy of SDSSJ0952+2143. The luminosity of Hβ, $L_{H\beta_n} = 10^{40}$ erg s^{-1}, can be used to estimate the emitting volume in dependence of gas density and temperature. Under photoionization Case B conditions (Osterbrock 1989), and assuming $T = 2 \times 10^4$ K, a density of $\log n = 2$ as in the [S II] emitting region (see Section 3.4) would imply an emitting volume with a size of $r = 50$ pc, while $\log n = 4$ implies $r = 2$ pc. The observed Hβ luminosity further implies a minimum rate Q of H-ionizing photons of $Q = 3.8 \times 10^{12} L_{H\beta_n} = 4 \times 10^{52}$ s^{-1} assuming full covering of the continuum source.

Narrow horns. Apart from the broad base and narrow core, the Balmer lines show a remarkable extra structure in form of two very narrow, unresolved, horns. These horns do not have any counterparts in any other emission lines, and our new NTT spectrum shows that they do vary between the 2005 SDSS observation and the 2008 NTT observation, and have become significantly fainter. The absence of the horns in other emission lines may be a consequence of high density. However, some coronal lines have very high critical density and are still not detected. Alternatively, the lines may form in collisionless shocks. These shocks produce strong hydrogen lines with a two-component profile consisting of a narrow component contributed by cold hydrogen atoms, and a broad component from hydrogen atoms that have undergone charge transfer reactions with hot protons while other optical forbidden lines are very faint (e.g., Raymond 1995; Heng & McCray 2007). The flux ratio of broad over narrow component depends on the shock velocity. In order to see whether there is extra components in the broad Balmer lines of SDSSJ0952+2143 matching the narrow horns, higher S/N observations are needed. The line shape (double-peaked profile) could arise in the case of two colliding streams of gas, in this case moving at a few hundred km s^{-1}, or alternatively in a two-sided jet or ring morphology or a bipolar outflow, and will be further discussed below.

3.3. Coronal Lines

Several flux ratios of emission lines of iron are of diagnostic value, since they are temperature and/or density sensitive (e.g., Nussbaumer & Storey 1982; Keenan & Norrington 1987). The ratio [Fe VII]3759/[Fe VII]6087 was used in Paper I for a first estimate of the temperature of the emitting gas. The ratio reported in Paper I was based on total line fluxes. Here we have decomposed both lines into a broad and a narrow component (Section 2.1.4) and remeasured the line ratio, which gives [Fe VII]3759/[Fe VII]6087 = 0.9 for the broad component and [Fe VII]3759/[Fe VII]6087 = 0.7 for the narrow component in 2005. These ratios imply gas temperatures in the range $T =$ 20,000–50,000 K for the gas which emits the broad component, and $T =$ 15,000–30,000 K for the gas which emits the narrow component (Keenan & Norrington 1987). [Fe VII]3759 could not be decomposed into two components in 2008. The inferred temperatures are consistent with a photoionization origin of the emission lines. Further, the widths of the narrow iron-line cores, of order ~200 km s^{-1} or less, argue against direct collisional ionization by shocks, since a minimum shock velocity of 300 km s^{-1} is required to collisionally ionize Fe^{10+} (Viegas-Aldrovandi & Contini 1989). This statement does of course not exclude the presence fast radiative shocks (Sutherland & Dopita 1995; Dopita & Sutherland 1996) which produce local ionizing radiation which can then photoionize low-velocity pre-shock gas. In that case, the degree of ionization would be higher in the ambient pre-shock gas than in the cooling post-shock gas. In situ production of the ionizing radiation also ensures efficient reprocessing into emission lines.

The ratio [Fe VII]5158/[Fe VII]6087 = 0.2 in 2005 implied an electron density $\log n_e =$ 6–7, while its decrease to [Fe VII]5158/[Fe VII]6087 < 0.06 in 2008 implies a higher density $\log n_e > 7$ (Keenan & Norrington 1987).[15] Further, it is reasonable to assume that the bulk of the iron emission lines should be emitted from gas below the critical density, which is 3×10^7 cm^{-3} for [Fe VII]6087, and ~ 10^9 cm^{-3} for [Fe X] and [Fe XI].

The 2008 line luminosity of [Fe VII]6087, 1.6×10^{40} erg s^{-1}, is almost as high as the simultaneously measured soft X-ray luminosity, implying that we either only see a fraction of the produced soft X-ray luminosity (the rest being completely absorbed), or that a strong EUV excess is present, or else that we still see the echo from a once brighter flare. Since the recombination timescale in the high-density coronal-line-emitting gas is very short (at $T = 2 \times 10^4$ K and $\log n = 7$, the hydrogen recombination timescale is on the order of 10 days), light travel time effects would then have to play a role.

3.4. [S II] Ratio

The emission-line intensity ratio [S II]6716/[S II]6731 is sensitive to density (Osterbrock 1989; Dopita & Sutherland 2003). The measured ratio, 1.3 in 2005 and 1.1 in 2008, indicates densities of $n \simeq 1 \times 10^2$ cm^{-3} and $n \simeq 3 \times 10^2$ cm^{-3}, respectively (at T = 10^4 K). [S II] therefore signals gas of much lower density than indicated by the coronal lines.

3.5. The Strength of [O III]4363/5007

The great strength of [O III]4363/5007 ≃ 0.2–0.3 in 2005 and 2008 significantly exceeds the value typically observed in Seyfert galaxies and is above photoionization predictions for a large parameter space (e.g., Figure 9 of Komossa & Schulz 1997; Groves et al. 2004). The observed value implies that we are beyond the low-density regime so that the ratio no longer only depends on temperature, but also becomes density sensitive (Osterbrock 1989; Dopita & Sutherland 2003). For a temperature of $T = (2-5) \times 10^4$ K the ratio implies a density on the order of $\log n = 7$ (Dopita & Sutherland 2003).

3.6. NIR Emission

Given that the 2MASS measurements most likely represent the host galaxy emission *prior* to the outburst we have used the NIR colors to determine the nature of the host galaxy. The values of $J - H = 0.9$ mag and $H - K_s = 0.1$ mag locate SDSSJ0952+2143 in the area typically populated by nonactive

[15] Note remaining uncertainties in the collision strengths of [Fe VII]; e.g., Section 3.3 of Ferguson et al. 1997.

Table 3
Summary of Some Key Parameters

Parameter	Measurement	Comment
X-ray luminosity	1×10^{41} erg s^{-1}	2008 *Chandra* (0.1–10 keV)
R magnitude	–20.8	2004 SDSS photometry
MIR luminosity	3.5×10^{43} erg s^{-1}	2008 *Spitzer* (10–20 μm)
Broad Hα luminosity	3×10^{41} erg s^{-1}	2005 SDSS spectrum
[Fe X]6375 luminosity	3.5×10^{40} erg s^{-1}	Brightest detected coronal line in 2005
[Fe VII]6087 luminosity	1.6×10^{40} erg s^{-1}	Brightest detected coronal line in 2008
Balmer decrement $H\alpha_b/H\beta_b$	12	2005 SDSS spectrum
SMBH mass	$7 \times 10^6\ M_\odot$	From stellar absorption features of the host galaxy; Paper I

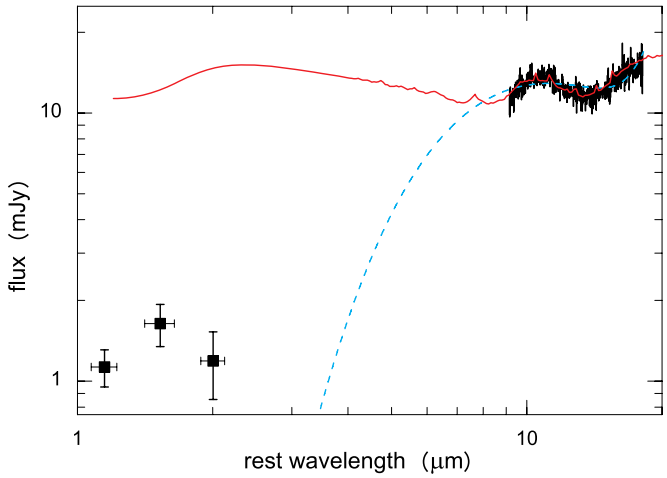

Figure 8. IR SED of SDSSJ0952+2143 observed with *Spitzer* and 2MASS (the latter consistent with GROND within an error of ∼0.5 mag). Overplotted is the mean *Spitzer* quasar SED (red; Netzer et al. 2007) and a simple two-component blackbody fit to the *Spitzer* data (blue).

(A color version of this figure is available in the online journal.)

galaxies in two-color diagrams (e.g., Hyland & Allen 1982; Willner et al. 1984; Glass & Moorwood 1985; Alonso-Herrero et al. 1996; our Figure 5).

3.7. MIR SED

The global *Spitzer* SED of SDSSJ0952+2143 indicates excess emission around 11 μm, and an increase at longer wavelengths, and closely resembles the mean PG quasar *Spitzer* IRS SED of Netzer et al. (2007; their Figure 3). The bumps in those quasar spectra are traced back to silicate emission (see also Schweitzer et al. 2006, and references therein). The extrapolation of the observed *Spitzer* MIR SED falls well above the NIR emission (dominated by the extended host) by an order of magnitude (Figure 8), implying that the IR emission of SDSSJ0952+2143 is completely dominated by relatively cold dust—unlike quasar spectra which commonly show a significant emission component around a few μm from relatively hot dust, heated by the radiation from the AGN accretion disk. The observed MIR emission is extraordinary luminous, with $L_{10-20\,\mu\mathrm{m}} = 3.5 \times 10^{43}$ erg s^{-1} in the narrow IRS SH band. The relatively low mass of the SMBH of the host galaxy of SDSSJ0952+2143, $M_{\mathrm{BH}} \simeq 7 \times 10^6\ M_\odot$ (Paper I; see our Table 3), implies that the observed 10-20 μm luminosity is already 1/25 of the Eddington luminosity.

With only one MIR spectrum at hand and no imaging information, there is currently two possibilities to explain the MIR emission. Either we see *temporary* emission from dust heated by the flare, or else this is *permanent* emission from a starburst region. The observed MIR luminosity is comparable to that of nearby IR selected Seyfert galaxies (e.g., Tommasin et al. 2008), so quite luminous. At the same time, we do not see evidence for a young stellar population in the optical spectrum. So, if the MIR emission was permanent, the starburst region would then have to be completely obscured in the optical band.

Within the limits of the blackbody approximation, we can estimate the size of the emission region. For the given blackbody temperature and MIR luminosity, we obtain a radius of the emission region of 0.5 pc.

We do not have tight constraints on the geometry of the dust distribution. However, the lack of reddening of the narrow Balmer lines implies that the dust is not in a spherical shell around this line-emitting region; and the strength of the coronal lines implies that this region is free of silicates, otherwise Fe would be heavily depleted onto dust grains.

4. DISCUSSION

4.1. Outburst Mechanisms

The strong emission-line and the low-energy continuum variability of SDSSJ0952+2143 are the consequence of a high-energy outburst which was itself not observed. The emission-line and continuum variability encompassing several wavebands and forbidden and allowed emission lines are unique among variability associated with the cores of galaxies.

Several different outburst mechanisms can potentially produce the very unusual emission-line signatures of SDSSJ0952+2143. We briefly introduce them in this section, and then come back to each of them in more detail in the following subsections. (1) An accretion disk around a SMBH will produce ionizing radiation that is reprocessed by surrounding gas clouds into characteristic broad and narrow emission lines which are commonly observed in the spectra of AGNs (Osterbrock 1989). Changes in the accretion rate, for instance, in form of a disk instability could lead to highly variable continuum emission and excite the unusual emission lines (Section 4.2). (2) A flare of electromagnetic radiation can be produced from the temporary accretion disk formed by the debris of a star tidally disrupted by a SMBH in the core of SDSSJ0952+2143. As the ionizing radiation travels through the nucleus, emission lines originate in the ISM and also in part of the stellar debris itself (Section 4.4). (3) A fraction of SNe emit significant X-ray radiation, which likely originates in shocks driven into the CSM by the SN ejecta. This radiation ionizes ambient gas, including the SN ejecta, the (clumpy) progenitor wind and the ISM. These components then emit broad and sometimes also narrow emission lines (Section 4.3). A small fraction of SN spectra

look surprisingly similar to those of AGNs (e.g., Figure 6 of Filippenko 1989, Figure 1 of Terlevich & Melnick 1988), even though essentially all AGNs and SN spectra look very different from SDSSJ0952+2143.

Finally, there is a region of parameter space where the mechanisms (1)–(3) discussed above overlap; including SNe exploding in gas-rich AGN cores, stellar tidal detonations, and flung-out stellar tidal debris interacting with the ISM (Section 4.5).

4.2. AGN Outburst

Some fraction of all AGNs show coronal line emission in their optical spectra (e.g., Seyfert 1943; Penston et al. 1984; Oliva et al. 1994; Binette et al. 1997; Nagao et al. 2000; Mullaney & Ward 2008). The large majority of these coronal lines are constant or, very rarely, show slight variability (e.g., Netzer 1974; Veilleux 1988). Only one, the active galaxy IC3599 (Brandt et al. 1995; Grupe et al. 1995; Komossa & Bade 1999), has shown strong transience in its coronal lines. In response to a luminous X-ray flare, several bright emission lines appeared and then faded on the timescale of years. The total amplitude of variability is large and the X-ray spectrum is very soft, both in high state and low state (Brandt et al. 1995; Grupe et al. 1995; Vaughan et al. 2004). A change in accretion rate (perhaps due to a disk instability or due to stellar tidal disruption) is a likely explanation of these observations (Brandt et al. 1995; Grupe et al. 1995).

Clearly, with its strong coronal lines and dramatic line variability, SDSSJ0952+2143 is different from AGNs in general, and is more extreme than IC3599 in its broadband emission-line and continuum response.

If a high-amplitude outburst occurred in an AGN, different emission-line regions—the broad line region (BLR), coronal line region (CLR), and narrow line region (NLR) – would be illuminated at different times, and will respond with different recombination timescales. Consequently, "outburst spectra" could look significantly different from equilibrium spectra. The range of densities inferred from the emission-line spectrum of SDSSJ0952+2143 is consistent with indications for local density inhomogeneities in the classical NLR of AGNs (e.g., Komossa & Schulz 1997; Brinkmann et al. 2002).

As noted in Paper I, the ratio [O III]/H$\beta_n \simeq 3$ formally places SDSSJ0952+2143 at the border between AGNs and LINERs in diagnostic diagrams; but given the variability of most or all emission lines, this cannot at all be used as a classification of the galaxy.[16] In terms of emission-line ratios, the classification of SDSSJ0952+2143 as active or inactive galaxy in quiescence therefore remains unknown at present.

However, the pre-flare 2MASS colors indicate a nonactive galaxy, the low-state X-ray flux measured with *Chandra* does not hint at the presence of a permanent AGN (except possibly a low-luminosity AGN), and the optical spectrum barely has a detectable nonstellar component. We therefore consider the presence of a classical AGN at the core of SDSSJ0952+2143, which underwent an unusual outburst, very unlikely.

[16] If we momentarily assume that the [O III] emission is permanent and use the known correlation between [O III] luminosity and X-ray luminosity among AGNs of Heckman et al. (2005; see also Netzer et al. 2006), we predict a (2–10) keV X-ray luminosity of $L_{2-10} \sim 10^{42}$ erg s^{-1}, higher than observed by more than one order of magnitude.

4.3. Supernova Explosion

4.3.1. Supernovae of Type IIn

One subclass of supernovae, those of type IIn (Schlegel 1990) show narrow emission lines preferentially from hydrogen and helium in their optical spectra in addition to broad lines (see Filippenko 1997 for a review; his Figure 14).[17] These lines are interpreted as a result of strong interaction of the SN ejecta with dense CSM (e.g., Chugai 1990; Chugai & Danziger 1994). Only a few SNe are known which exhibit coronal lines (e.g., SN 1988Z: Turatto et al. 1993, SN 1993J: Garnavich & Ann 1994, SN 1995N: Fransson et al. 2002; SN 1987A: Gröningsson et al. 2008, SN 1997eg: Hoffman et al. 2008, SN 2005ip: Smith et al. 2009) and detection of ionization states as high as [Fe XIV] is very rare. According to Smith et al. (2009), SN 2005ip is unprecedented in the way the coronal lines dominate the optical spectrum of that SN.

Several SNe IIn are also relatively X-ray luminous, exceeding 10^{40} erg s^{-1} (e.g., SN 1988Z: Fabian & Terlevich 1996; Aretxaga et al. 1999; Schlegel & Petre 2006; SN 1986J: Bregman & Pildis 1992; Temple et al. 2005; SN 2006jd: Immler et al. 2007; see Schlegel 1995, 2006, and Table 1 of Immler 2007[18] for overviews). Strong ionizing radiation may originate from the shock break-out, Compton-upscattering, and in shocks when SN ejecta collide with the precursor wind and/or the ISM. A number of type IIn SNe show excess emission in the NIR, plateaus in their NIR light curves, and characteristic variability of their Balmer-line profiles. These properties have been traced back to the presence of dust, either pre-existing dust which is heated collisionally or radiatively after the SN explosion, or newly formed dust which coagulated after the SN explosion in cool, dense regions (e.g., Merrill 1980; Lucy et al. 1989; Roche et al. 1989; Moseley et al. 1989; Wooden et al. 1993; Gerardy et al. 2002; Pozzo et al. 2004; Sugerman et al. 2006; Meikle et al. 2006; Smith et al. 2008b; Fox et al. 2009 and references therein).

There are several key sites of emission line formation. The radiation produced in the shocks will ionize the surrounding ISM, the stellar wind of the SN precursor and the high-density SN ejecta themselves. The narrow lines likely arise in the CSM (sometimes in the ISM); while broad lines likely come from the SN ejecta (e.g., Chugai & Danziger 1994; Filippenko 1997). Generally, SNe of type IIn show substantial heterogeneity with respect to their luminosities and emission-line properties. They are relatively rare, comprising only a few percent of all core-collapse SNe (Gal-Yam et al. 2007; Smartt et al. 2009).

4.3.2. Superluminous Iron Lines, and Comparison with SN 2005ip and SN 1988Z

Given similarities of the optical spectra of SDSSJ0952+2143 first presented in Paper I with the recently published remarkable spectra of the type IIn supernova SN 2005ip (Smith et al. 2009; S09 hereafter), we consider an origin of SDSSJ0952+2143 in terms of a similarly unusual supernova. S09 reported very

[17] SNe of this type are, e.g., SN 1987F (Wegner & Swanson 1996), SN 1988Z (Stathakis & Sadler 1991; Turatto et al. 1993; Aretxaga et al. 1999), SN 1995G (Pastorello et al. 2002), SN 1995N (Fransson et al. 2002), SN 1994W (Chugai et al. 2004), SN 1997eg (Hoffman et al. 2008), SN 1998S (Leonard et al. 2000), SN 2005gl (Gal-Yam et al. 2007), SN 2006tf (Smith et al. 2008a), and SN 1997cy (Germany et al. 2000; Turatto et al. 2000). We note in passing that SNe associated with GRBs are typically of type Ic which lack hydrogen features in their optical spectra.

[18] See http://lheawww.gsfc.nasa.gov/users/immler/supernovae_ list.html maintained by S. Immler for updates.

strong coronal lines including a large number of transitions, and ionization states up to [Fe XIV], with a peak luminosity (at day 93) in [Fe XIV] of 1.5×10^{38} erg s^{-1}. SN 2005ip and several other type IIn SNe also show high ratios of [O III]4363/[O III]5007, broad Balmer lines with widths of at least (one–several) thousand km s^{-1} and very high Balmer decrements (up to 25 in the case of SN 2005ip). The peak luminosity of SN 2005ip was only modest with an (unfiltered) absolute magnitude of –17.4 (S09).

SDSSJ0952+2143 is phenomenologically similar in several of its emission-line properties, especially line ratios, but much brighter in the optical, and brighter in X-rays, and, in particular, much more luminous in the coronal lines. According to S09, SN 2005ip is the SN with the strongest iron coronal lines, in the way they dominate the spectrum of that SN. The luminosity in the high-ionization coronal lines of SDSSJ0952+2143 is a factor of $\sim$ 100 higher than the highest value measured in SN 2005ip (S09) and in SN 1988Z (Turatto et al. 1993) and it is a factor 10^3 higher than in SN 1995N (Fransson et al. 2002), and a factor 10^4 higher than in SN 1993J (Garnavich & Ann 1994).[19]

In the context of an SN interpretation, SDSSJ0952+2143 therefore is the SN with the most luminous iron coronal lines. SDSSJ0952+2143 is also among the very luminous SNe II in terms of continuum emission (cf. Figure 3 of Smith et al. 2008a), with an R magnitude of –20.8 mag in 2004 (including emission from the host galaxy, but likely dominated by the transient), and it almost rivals the "hypernova" SN1997cy (Turatto et al. 2000; Pastorello et al. 2002) in its large Hα luminosity. In the context of the SN scenario, the density of the forbidden line-emitting gas of SDSSJ0952+2143, $\log n \simeq 2...7$, is consistent with a clumpy progenitor wind and/or ISM (but could also imply SN explosion into a star-forming region), the lowest-velocity gas with the pre-shock wind speed of an LBV progenitor (e.g., Humphreys & Davidson 1994; Smith et al. 2008a).

On the other hand, there are also significant spectral differences between SDSSJ0952+2143 and SN 2005ip (and other similar SNe); for instance, (1) no He I transitions are detected in our spectra; neither broad nor narrow, whereas they are frequently seen in SNe. (2) The narrow horns in the Balmer lines of SDSSJ0952+2143 are unusual (but see below). (3) The profile asymmetry of Hα of SDSSJ0952+2143 is opposite to that sometimes seen in SNe (which show apparent blueshifts; often traced back to stronger extinction in the red part of the line from the far side of the SN ejecta; e.g., Lucy et al. 1989, S09).

Regarding the narrow horns in the Balmer lines, it is interesting to note a potential similarity with SN 1998S, which showed a double-horned profile (Garnavich et al. 1998), traced back by Gerardy et al. (2000) to the presence of interacting dense clumpy circumstellar gas with a ring-like morphology. However, they measured the three peaks at velocities of -4900, -400 and +3300 km s^{-1}, at much wider velocity separation than the peaks of SDSSJ0952+2143. The lines are also much broader in SN 1998S.

4.3.3. Luminous X-ray Emission

Chandra indicates a relatively hard X-ray spectrum of SDSSJ0952+2143, frequently seen in SNe (thermal spectra with temperatures of several–10 keV). The observed X-ray luminosity of SDSSJ0952+2143 is higher than that of most other known SNe. Only $\sim$40 SNe are X-ray detected at all (according to Table 1 of Immler 2007, and adding recent detections) and only a handful of them are more luminous than 10^{40} erg s^{-1}. One of the most luminous (long-duration) X-ray emitting SNe is SN1988Z (Fabian & Terlevich 1996), at $L_{\rm x} \approx 10^{41}$ erg s^{-1}. SN 2005ip was detected at 1.6×10^{40} erg s^{-1} (0.2–10 keV, at day 461; Immler & Pooley 2007). If of SN origin, SDSSJ0952+2143 is one of the most distant X-ray detected, and one of the most X-ray luminous SNe known.

Perhaps the tightest constraints on any SN-based outburst scenario are set by the huge luminosities in the narrow emission lines. The luminosity in the highest ionization coronal lines implies very luminous intrinsic soft X-ray emission under photoionization conditions. So far, line luminosities $> 10^{40}$ erg s^{-1} as in SDSSJ0952+2143 have only been observed in AGNs (e.g., Nagao et al. 2000; Mullaney & Ward 2008). While the ionization potentials of [Fe VII]–[Fe XIV] (0.1–0.4 keV) fall in the X-ray regime, it is not straightforward to convert the observed coronal line luminosities into X-ray luminosity, since two processes contribute to the line excitation, collisional excitation and resonance fluorescence by UV photons (e.g., Osterbrock 1969), and since atomic parameters are still relatively uncertain (e.g., Pelan & Berrington 1995; Mohan et al. 1994; Oliva 1997; Berrington 2001). In AGNs, the observed coronal line luminosity is approximately 0.1% (to 1%) of the observed X-ray luminosity. If the line formation efficiency was similar under SN conditions, in the case of SDSSJ0952+2143 this would imply an intrinsic soft X-ray luminosity on the order of at least $\sim 10^{42-43}$ erg s^{-1}. No such X-ray luminous SN has ever been observed (or identified as such; the luminous X-ray emission of SN 2008D only lasted for seconds-minutes; Soderberg et al. 2008). An SN explosion into a dense medium (Wheeler et al. 1980; Shull 1980) was invoked to explain the luminous X-ray emission of SN 1988Z (Fabian & Terlevich 1996), but it is very difficult to reach luminosities of 10^{42-43} erg s^{-1} by this mechanism (Komossa & Bade 1999).

4.3.4. Luminous IR Emission

Few SNe have MIR measurements and spectroscopy in particular (e.g., Kotak et a. 2006; Gerardy et al. 2007). SN 1987A is the best-studied exception (e.g., Roche et al. 1989; Moseley et al. 1989; Wooden et al. 1993). Its MIR SED is relatively flat, indicating that it is dominated by an almost featureless dust component (Wooden et al. 1993), perhaps graphite (Moseley et al. 1989). The characteristic structure of the *Spitzer* spectrum of SDSSJ0952+2143 indicates the presence of silicates. The MIR emission is extraordinarily luminous, with at least $L_{10-20\,\mu{\rm m}} = 3.5 \times 10^{43}$ erg s^{-1}. This compares to other IR luminous SNe which only reached up to several 10^{40-41} erg s^{-1} in the NIR (e.g., Gerardy et al. 2002; Pozzo et al. 2004), while the most luminous SNe ever observed reached peak luminosities of few $\times 10^{44}$ erg s^{-1} in the optical band (e.g., Quimby et al. 2007).

The blackbody radius inferred from the MIR emission of SDSSJ0952+2143 (Section 3.7) corresponds to 0.5 pc. This is much larger than the distance, the SN ejecta could have traveled within several years and implies that we see an IR light echo of pre-existing dust. The huge MIR luminosity raises the question whether we instead see permanent emission from a dusty star-forming region. We cannot entirely rule out this possibility, but it is unlikely because a luminosity of similar magnitude was inferred from the presence of the [Fe VII] coronal lines in the

[19] Note that only few spectra of SDSSJ0952+2143 exist; its peak line luminosity could have therefore been even higher.

previous section, and this (UV–X-ray) radiation is a plausible heating source of the dust. We therefore expect that the dust emission maximum continues to shift further toward the FIR as the dust cools and the incident radiation fades away. A new IR observation with *Spitzer* or the *Herschel Space Observatory* would allow us to check whether this trend indeed exists.

4.3.5. Location and Environment

A dense environment of SNe of type IIn is usually invoked to explain the luminous continuum radiation of several of these SNe, and is also inferred from emission-line characteristics. The densities we derive are consistent with such an interpretation. A dense environment of SDSSJ0952+2143 is also consistent with the strong MIR light echo from dust, and with the location of the transient within the galaxy core where dense gas is plausibly most abundant. At the same time, the blueness of the optical power-law continuum and the *GALEX* colors argue against heavy extinction along the line of sight. This would then locate the event at the edge of a molecular cloud complex, where most dust directly along our line of sight was destroyed by the bright flare. Finally, we note that the evidence for spiral structure in the GROND images is not inconsistent with a SNII interpretation; type IIs have not yet been observed in elliptical galaxies (Capellaro et al. 1999).

4.4. Transient Accretion Event in a Nonactive Galaxy

Given the extreme luminosity requirements in the context of an SN scenario, we now return to accretion power as energy source. Since there is no evidence for classical permanent AGN activity in SDSSJ0952+2143 in the form of a permanent optical and X-ray bright accretion disk, we focus now on the possibility of a temporary accretion event in a nonactive galaxy, for instance by accretion of a molecular cloud or the tidal disruption of a star. These events could similarly happen in a low-luminosity AGN the presence of which we cannot yet exclude. In the latter, an accretion disk instability could also temporarily enhance the accretion luminosity. That said, we mostly concentrate on the tidal disruption scenario in what follows.

Interestingly, all of the observed emission-line and continuum properties can also potentially be understood in the context of a stellar tidal disruption event; where a star is disrupted in a gas-rich core environment.

4.4.1. Tidal Disruption of a Star by a SMBH

A star approaching a SMBH will be tidally disrupted once the tidal forces of the SMBH exceed the star's self gravity. A fraction of the stellar debris will subsequently be accreted, producing a luminous flare of radiation (e.g., Hills 1975; Young et al. 1977; Gurzadian & Ozernoi 1981; Luminet 1985; Rees 1988; Evans & Kochanek 1989; Laguna et al. 1993; Li et al. 2002; Gomboc & Cadez 2005; Ivanov & Chernyakova 2006; see Komossa 2002 for a much longer list of references on theoretical aspects of tidal disruption) peaking in the X-rays or UV and lasting on the order of months to years.

X-ray variability, up to factors of ∼6000, has been almost exclusively detected in nonactive galaxies, and these events represent the best observational evidence to date for the process of tidal disruption of stars by SMBHs (e.g., Komossa & Bade 1999; Halpern et al. 2004; Komossa et al. 2004). The tidal disruption candidates reached huge X-ray luminosities up to at least $L_{\rm sx} \approx 10^{44}$ erg s^{-1} and show a light curve which jointly declines as $t^{-5/3}$, as predicted in some variants of tidal disruption models (e.g., Rees 1990). A few events in the UV shared similar properties with these X-ray events (similar decline law based on well covered light curves, possibly soft X-ray spectrum, and (much lower) UV amplitude of variability of a factor of a few) and were thus interpreted along the same lines (Gezari et al. 2008; see also Renzini 2001; Stern et al. 2004). None of the tidal disruption flares so far observed from nonactive galaxies had an emission-line "light echo" detected, but optical follow-up spectroscopy has typically only been obtained several years after the flare (Komossa & Bade 1999; Komossa & Greiner 1999; Grupe et al. 1999; Greiner et al. 2000; Gezari et al. 2003, 2008; Esquej et al. 2008; Cappelluti et al. 2009).[20]

Apart from the accretion of stellar debris which causes the powerful X-ray flares, in the course of a tidal disruption event, ionizing radiation will also be released in shocks during stream-stream collisions (Kato & Hoshi 1978; Rees 1988; Lee et al. 1996), and during collisions of the ejected stellar debris with the ISM (Kokhlov & Melia 1996; Ayal et al. 2000).

4.4.2. Emission-Line Light Echoes

The radiation from accretion and other processes will ionize any surrounding gaseous matter in the galaxy core: (1) the ISM of the host galaxy, including the gas clouds of BLR, NLR, CLR, and torus, if present, and (2) the gaseous debris of the star itself which would be of very high density, show a spread in densities, have asymmetric spatial distribution, and may well have an unusual chemical composition.

A tidal disruption flare would therefore enable an extreme application of "reverberation mapping" where all gaseous material responds to one single flare (Blandford & McKee 1982) rather than a complicated light curve. This is of special interest with application to the cores of active galaxies, for instance to map the response of the molecular torus. It is also of interest with respect to nonactive galaxies, because it would tell us which of those gaseous components typically detected in active galaxies (like the BLR) are still present in nonactive galaxies. Once applied to a large number of galaxies, this method might also provide a new route of addressing the nature and velocity field of the gas that fuels SMBHs.

Predictions of how emission-line spectra excited by tidal disruption flares should look like in detail, do not yet exist and are complicated by the time dependence of the ionization; early spectra would be dominated by high-ionization emission lines, while lines like He II and some low-ionization lines would persist especially long (e.g., Binette & Robinson 1987) after the flare, when [O III]5007 has already faded.[21]

After the tidal disruption of a star, streams of tidal debris would form, spreading over a number of orbits. This would result in complex multipeaked Balmer emission-line profiles in the early phase of disruption (days to months; Bogdanovic et al. 2004). After that, line profiles would change less rapidly,

[20] A few events of unusual broad line variability in AGNs and LINERs have sometimes been linked to accretion events including tidal disruption: for instance, the transient broad double-peaked Balmer lines of NGC 1097 (Storchi-Bergmann et al. 1995; Eracleous et al. 1995; Storchi-Bergmann et al. 2003) and the transient broad He II line of NGC 5548 (Peterson & Ferland 1986). We also note that faint high-ionization [O III] emission detected in the post-flare *HST* spectrum of NGC 5905 (Gezari et al. 2003) could have well been excited by the flare, rather than representing permanent low-level activity.

[21] Photoionization modeling of the coronal lines of the flaring galaxy IC3599 has shown that gas with a density of 10^9 cm^{-3} and a column density of 10^{23} cm^{-2} (conditions similar to the outer BLR or CLR in AGNs) can produce the observed line ratios (Komossa & Bade 1999). In addition, the strong soft excesses seen in tidal disruption candidates (Komossa 2002) boost the coronal lines in strength.

and would represent a superposition of different components of the tidal debris, which would respond to the time-dependent illumination from the central accretion disk. Simulations of the stellar disruption process (e.g., Evans & Kochanek, Laguna et al. 1993; Ayal et al. 2000; Gomboc & Cadez 2005) have shown that approximately 75% of the stellar debris is unbound after first pericenter return. The innermost bound debris circularizes quickly, while the rest is spread over a number of eccentric orbits. Such a configuration might explain the broad component in Hα and its peak shift on the timescale of years, while the high density of the stellar debris would explain the large Balmer decrement. At the same time, the line luminosity cannot easily be explained within this scenario (see Section 3.2). Stream-stream collisions between returning debris and more tightly bound gas might produce double-horned profiles like the one we observe (see the discussion on collisionless shocks in Section 3.2), but we would expect much stronger profile variability on the timescale of years than is actually observed (while the narrow horns of SDSSJ0952+2143 do vary in intensity, the velocity separation of the two peaks did not change within the errors). Alternatively, the double-horned emission could represent narrow streams of unbound debris (viewed from a special direction, since line centroid shifts are small). Other geometries which could produce double-horned profiles involve a jet or bipolar outflow component; the small line width and peak separation would require a special viewing angle.

The unbound stellar tidal debris will be flung out from the system at high speed and when interacting with the ISM could cause effects similar to a supernova remnant (SNR) but much more powerful (Khoklov & Melia 1996). While the available kinetic energy could be much higher than in a SN, the mechanism only works efficiently if the escaping debris forms a narrow stream rather than a broad fan (see the discussion in Khoklov & Melia 1996).

The estimated radius of the IR light echo, 0.5 pc, is consistent with the expected location of molecular gas in the galaxy core. Based on the black hole mass of the host galaxy, and applying typical scaling relations known in active galaxies (Elitzur 2007), the inferred size of the emission region is comparable to the molecular torus. Any dust mixed with gas at distances much closer to the nucleus would have been destroyed by the bright flare. The fact that we see silicate emission rather than absorption features further implies that we have a relatively unobscured view into the galaxy.

4.4.3. Overall Energetics

Tidal flares might be well powered by Eddington-limited accretion shortly after the disruption. Assuming a $t^{-5/3}$ decline law (e.g., Rees 1990; Komossa & Bade 1999) for the luminosity evolution after disruption, and extrapolating backward in time starting with the observed X-ray luminosity in 2008, the predicted luminosity is still below the Eddington luminosity in 2004, consistent with tidal disruption. Given uncertainties in the decline law and the EUV part of the continuum, this estimate is uncertain by at least one order of magnitude. We note in passing that the observed X-ray spectrum of SDSSJ0952+2143 is much harder than the previously observed, very soft, tidal flares (e.g., Komossa & Bade 1999).

4.5. Links Between Supernovae, Tidal Disruption, and GRBs

There might well be a region of parameter space where the mechanisms discussed in previous sections are related: It has long been pointed out, and reconfirmed in recent studies, that high penetration factors of stars approaching SMBHs could ignite nuclear burning in the stellar core (including especially white dwarfs) and thus trigger an SN explosion[22] (e.g., Carter & Luminet 1982; Bicknell & Gingold 1983; Luminet & Marck 1985; Luminet & Pichon 1989; Frolov et al. 1994; Dearborn et al. 2005; Brassart & Luminet 2008; Rosswog et al. 2008). In that case, the collisions of the ejected stellar debris with the ISM could be even more powerful than in a classical SNR (Khoklov & Melia 1996). Variants of tidal disruption and detonation have also been employed to explain certain classes of GRBs (e.g., Carter 1992; Lu et al. 2008; Brassart & Luminet 2008). Among the GRBs, a few appear to be associated with SNe (of type Ic) (e.g., SN 1988bw/GRB980425: Galama et al. 1998, SN 2003dh/GRB030329: Hjorth et al. 2003; SN 2006aj/GRB060218: Mazzali et al. 2006; see Woosley & Bloom 2006 for a review).

We have checked the data base[23] of well localized (better than 1°) GRBs since 1997 in order to see whether any GRB was recorded from the direction of SDSSJ0952+2143. This includes GRB detections by HETE II, BeppoSAX, INTEGRAL, *Swift*, AGILE, Fermi-LAT, and the Interplanetary Network. None was found within 10°. However, we note that the temporal coverage of the field was below about 25%. SN (in dense media) and GRB-related models have also been discussed by Komossa & Bade (1999) for the tidal disruption candidate NGC 5905, but were not favored.

Another interesting phenomenon is a SN exploding in an "AGN-like" gaseous core, e.g., in or near a BLR or NLR cloud, or the molecular torus. This would complicate emission-line modeling, and if not identified as such could lead to wrong conclusions about the properties of the wind of the progenitor star.

At present, the similarities in several spectral properties of SN 2005ip and SDSSJ0952+2143 suggest a similar mechanism at work; and the overall appearance of SN 2005ip suggests a classical SN explosion, albeit with a number of peculiarities.

While it is important to keep in mind potentially large similarities between SN "light echoes" and tidal disruption "light echoes," at present the SN scenario perhaps is the most conservative interpretation of SDSSJ0952+2143—even though the coronal line luminosity and the MIR luminosity is spectacular and unprecedented.

Other very peculiar iron coronal lines in AGNs might have an SN origin, too (while the bulk of AGN coronal lines are spatially extended and have properties which are best explained by classical models of the coronal line region).

4.6. Event Rate

In order to estimate the rate of events as unusual as SDSSJ0952+2143, we have started a systematic search for similar objects among 7×10^5 galaxies of the SDSS galaxy data base. A first quick-look study produced at least two more events which fulfill the following three criteria: (1) [Fe VII]–[Fe XI] comparably strong as [O III]5007; (2) large Fe line luminosities; and (3) detection of Fe line variability in our follow-up optical spectroscopy (H. Zhou et al. 2009, in preparation; S. Komossa et al. 2009, in preparation). All three events arise from the galaxy cores within the errors. There may be more such objects, but

[22] Most of these events would occur strictly in galaxy *cores* even though tidal disruption/detonation of stars around recoiling SMBHs (Komossa & Merritt 2008) and white dwarf tidal detonation by intermediate-mass BHs (Rosswog et al. 2008) could happen offnuclear.

[23] http://www.mpe.mpg.de/~jcg/grbgen.html

taking those three safely identified so far results in a *lower limit* on the event rate of 4×10^{-6}/galaxy/("a few" years). The exact value of "a few" depends on the longevity of the iron features which could be on the order of 0.5–5 years. This rate compares to theoretical predictions of the tidal disruption rate of $\sim 10^{-5}$/galaxy/year (Merritt 2009), and to observational constraints on this rate which are on the same order (Donley et al. 2002; Esquej et al. 2008).

4.7. Future Follow-up Observations

A number of future observations are of interest in further distinguishing between different scenarios for SDSSJ0952+2143. Several type II SNe turned out to be luminous radio emitters (e.g., Weiler et al. 1990; van Dyk et al. 1993), while in the context of stellar tidal disruption it is still unknown whether these events will produce significant radio emission. Radio follow-ups are therefore of interest. X-ray monitoring will tell the long-term decline law. While all tidal disruption candidates showed a continuous fading of their X-ray light curves (Komossa 2002), supernovae have more complicated X-ray light curves which can strongly increase or decrease with time (Schlegel 2006; Immler 2007). A new *GALEX* or *Swift* observation should confirm the fading of the UV emission. An optical image of subarcsecond resolution would allow accurate localization of the faint continuum source within the galaxy core. Optical spectroscopic monitoring of the broad and narrow emission lines will provide the best diagnostic of the line-emitting gas. Among all spectral features of SDSSJ0952+2143 three stand out as special. (1) The narrow horns in the Balmer lines; luminous, with small kinematic separation, and very small line widths (< 200 km s^{-1}). High S/N observations would much better resolve the profile, and its temporal evolution. (2) The ultraluminous coronal lines. [Fe VII]6087 is still luminous and persistent in the most recent spectra, and measurement of its longevity will give tight constraints on the power source of the line emission, and therefore on the outburst mechanism. (3) The huge MIR luminosity of at least 3.5×10^{43} erg s^{-1}. One more *Spitzer* or a *Herschel* observation would tell whether this emission is permanent or varies in luminosity and temperature, and is therefore definitely related to the flare.

5. SUMMARY AND CONCLUSIONS

After the initial detection of the exceptional optical emission-line spectrum of SDSSJ0952+2143 and its variability (Paper I), and suspecting a tidal disruption event, peculiar AGN or supernova explosion, we have carried out multiwavelength follow-up observations, employing *Spitzer*, *Chandra*, NTT, the Xinglong telescope, and GROND, in combination with archival observations with *ROSAT*, *XMM-Newton*, *Swift*, 2MASS, NVSS, and *GALEX*.

SDSSJ0952+2143 shows the following continuum and emission-line properties.

1. The 2MASS colors (likely pre-flare) indicates a nonactive galaxy.
2. The observed X-ray luminosity of 10^{41} erg s^{-1} in 2008 is below that of a typical AGN and above a typical SN.
3. The optical spectrum of SDSSJ0952+2143 is dominated by luminous coronal lines, and those of the highest ionization have dramatically faded between 2005 and 2008.
4. The wide range in ionization states and critical densities of the forbidden emission lines and several density-sensitive line ratios indicate a range in electron densities of the line-emitting gas ($\log n = 2...7$). The temperature-sensitive line ratios imply photoionization as dominant ionization mechanism.
5. The luminosity in each of the high-ionization lines [Fe VII]6087, [Fe X], [Fe XI] and [Fe XIV] is extraordinary and exceeds 10^{40} erg s^{-1} in 2005. It persists in [Fe VII] for at least three years. Depending on the efficiency of reprocessing UV–X-ray radiation into coronal lines, this implies an intrinsic luminosity of at least 10^{42-43} erg s^{-1}.
6. At least three to four different kinematical components are present in the optical spectrum, with FWHMs in the range $<$200–2000 km s^{-1}.
7. The narrow Balmer lines are triple-peaked with two remarkable unresolved horns which do not have a counterpart in any other emission line, possibly the signature of collisionless shocks.
8. The *Spitzer* SED shows a ~ 10 μ bump and a rise toward longer wavelengths, reminiscent of emission by warm silicate dust. It shares some similarity with the average *Spitzer* PG quasar SED. However, the NIR falls short of the extrapolated MIR SED by one order of magnitude, unlike quasar spectra. For few, if any, of such extreme transients as SDSSJ0952+2143, MIR spectroscopy was ever done.
9. The MIR luminosity is huge and amounts to at least $L_{10-20\,\mu\mathrm{m}} = 3.5 \times 10^{43}$ erg s^{-1} at the time of the *Spitzer* observation. The inferred blackbody radius of 0.5 pc implies that we see an IR light echo from pre-existing dust.

Taken together, these data paint the picture of a very energetic outburst of radiation in the inner 1.5 kpc of the galaxy SDSSJ0952+2143. The high-energy part of this flare was not observed directly, but we did see the reprocessing of this radiation into emission lines, and the low-energy continuum variability.

There are two possible explanations for the radiation outburst: a tidal disruption/accretion event onto the SMBH of a nonactive or mildly active galaxy, or an extreme supernova explosion. Since only one single AGN previously showed high-amplitude variability in its iron coronal lines and no known nonactive galaxy has shown this phenomenon, a rigorous comparison with known object classes can only be done for SNe. Since there appears to be nothing in the spectrum of SDSSJ0952+2143 which differs enough from a few known extreme SNe, we cannot exclude an SN interpretation. If an SN, SDSSJ0952+2143 is the most distant, and most X-ray and MIR luminous, X-ray detected SNIIn; and the most luminous known in high-ionization iron coronal lines. An extreme accretion flare in a low-luminosity AGN or nonactive galaxy, especially by stellar tidal disruption, remain possibilities at present and would produce potentially very similar emission-line spectra. The large observed iron coronal line luminosities are unprecedented among SNe and exceed previous record holders by a factor 100.

We thank Lee Armus, Dirk Grupe, Stefan Immler, Gottfried Kanbach, Jean-Pierre Luminet, Dieter Lutz, Ximena Mazzalay, Hagai Netzer, Nathan Smith, and Eckhard Sturm for very useful discussions, Thomas Krühler for running the GROND pipeline data reduction, and our referee for his/her insightful comments. Part of this research was carried out while M.D., S.K., A.R., and M.S. stayed at the Aspen Centre for Physics, and we thank the Centre for its support and hospitality. We acknowledge use of the SDSS, *GALEX*, 2MASS, NVSS, *ROSAT*, *Swift* BAT, and *XMM-Newton* data base and of NED and ADS.

We have acquired new data with ESO's NTT, the Xinglong telescope, GROND, *Spitzer* and *Chandra*. We thank all instrument teams, and especially the SDSS team for making available to the whole astrophysics community their outstanding data base on which the discovery of this galaxy was based. A.R. thanks Lee Armus for discussing the IRS data reduction. We acknowledge *Spitzer* grant P483. H.Z. acknowledges support from the Alexander von Humboldt Foundation, the Chinese Natural Science Foundation through CNSF-10533050, 10573015, the CAS knowledge innovation project No. 1730812341, and the national 973 project (2007CB815403). A.G. acknowledges support by the Israeli Science Foundation, an EU Seventh Framework Programme Marie Curie IRG fellowship, and the Benoziyo Center for Astrophysics, a research grant from the Peter and Patricia Gruber Awards, and the William Z. and Eda Bess Novick New Scientists Fund at the Weizmann Institute. D.X. acknowledges support from the Chinese National Science Foundation (NSFC) under grant NSFC 10873017, and from program 973 (2009CB824800).

REFERENCES

Adelman-McCarthy, J. K., et al. 2008, ApJS, 175, 297
Ajello, M., et al. 2008, ApJ, 678, 102
Ayal, S., Livio, M., & Piran, T. 2000, ApJ, 545, 722
Alonso-Herrero, A., Ward, M. J., & Kotilainen, J. K. 1996, MNRAS, 278, 902
Aretxaga, I., et al. 1999, MNRAS, 309, 343
Berrington, K. A. 2001, in ASP Conf. Ser. 247, Spectroscopic Challenges of Photoionized Plasmas, ed. G. Ferland & D. W. Savin (San Francisco, CA: ASP), 137
Bicknell, G. V., & Gingold, R. A. 1983, ApJ, 273, 749
Binette, L., & Robinson, A. 1987, A&A, 177, 11
Binette, L., Wilson, A. S., Raga, A., & Storchi-Bergmann, T. 1997, A&A, 327, 909
Blandford, R. D., & McKee, C. F. 1982, ApJ, 255, 419
Bogdanovic, T., et al. 2004, ApJ, 610, 707
Brandt, W. N., Pounds, K., & Fink, H. H. 1995, MNRAS, 273, L47
Brassart, M., & Luminet, J.-P. 2008, A&A, 481, 259
Bregman, J. N., & Pildis, R. A. 1992, ApJ, 398, L107
Brinkmann, A. C., et al. 2002, A&A, 396, 761
Capellaro, E., Evans, R., & Turatto, M. 1999, A&A, 351, 459
Cappelluti, N., et al. 2009, A&A, 495, L9
Carter, B. 1992, ApJ, 391, L67
Carter, B., & Luminet, J.-P. 1982, Nature, 296, 211
Chugai, N. N. 1990, Sov. Astron. Lett., 16, 475
Chugai, N. N., & Danziger, I. J. 1994, MNRAS, 268, 173
Chugai, N. N., et al. 2004, MNRAS, 352, 1213
Condon, J. J., et al. 1998, AJ, 115, 1693
Dale, D. A., et al. 2009, ApJ, 693, 1821
Dearborn, D. S. P., Wilson, J. R., & Mathews, G. J. 2005, ApJ, 630, 309
Devillard, N. 1997, The Eclipse Software, The Messenger, No 87
Donley, J. L., Brandt, W. N., Eracleos, M., & Boller, T. 2002, AJ, 124, 1308
Dopita, M. A., & Sutherland, R. S. 1996, ApJS, 102, 161
Dopita, M. A., & Sutherland, R. S. 2003, Astrophysics of the Diffuse Universe (Berlin: Springer)
Elitzur, M. 2007, in ASP Conf. Ser. 373, The Central Engine of Active Galactic Nuclei, ed. L. C. Ho & J.-M. Wang (San Francisco, CA: ASP), 415
Eracleous, M., Livio, M., & Halpern, J. P. Storchi-Bergmann 1995, ApJ, 438, 610
Esquej, P., et al. 2008, A&A, 489, 543
Evans, C. R., & Kochanek, C. S. 1989, ApJ, 346, L13
Fabian, A. C., & Terlevich, R. 1996, MNRAS, 280, L5
Filippenko, A. V. 1982, PASP, 94, 715
Filippenko, A. V. 1989, AJ, 97, 726
Filippenko, A. V. 1997, ARA&A, 35, 309
Fox, O., et al. 2009, ApJ, 691, 650
Fransson, C., et al. 2002, ApJ, 572, 350
Frolov, V. P., Khokhlov, A. M., Novikov, I. D., & Pethick, C. J. 1994, ApJ, 432, 680
Ferguson, J. W., Korista, K., & Ferland, G. 1997, ApJS, 110, 287
Galama, T. J., et al. 1998, Nature, 395, 670
Gal-Yam, A., et al. 2007, ApJ, 656, 372
Garnavich, P. M., & Ann, H. B. 1994, AJ, 108, 1002
Garnavich, P. M., et al. 1998, IAU Circ., 7058, 1
Gerardy, C. L., Fesen, R. A., Höflich, P., & Wheeler, J. C. 2000, AJ, 119, 2968
Gerardy, C. L., et al. 2002, ApJ, 575, 1007
Gerardy, C. L., et al. 2007, ApJ, 661, 995
Germany, L. M., Reiss, D. J., Sadler, E. M., Schmidt, B. P., & Stubbs, C. W. 2000, ApJ, 533, 320
Gezari, S., Halpern, J., Komossa, S., Grupe, D., & Leighly, K. 2003, ApJ, 592, 42
Gezari, S., et al. 2008, ApJ, 676, 944
Glass, I. S., & Moorwood, A. F. M. 1985, MNRAS, 214, 429
Gomboc, A., & Cadez, A. 2005, ApJ, 625, 278
Greiner, J., Schwarz, R., Zharikov, S., & Orio, M. 2000, A&A, 362, L25
Greiner, J., et al. 2008, PASP, 120, 405
Gröningsson, P., et al. 2008, A&A, 492, 481
Groves, B. A., Dopita, M. A., & Sutherland, R. S. 2004, ApJS, 153, 75
Grindlay, J., et al. 1976, ApJ, 205, L127
Grupe, D., Thomas, H.-C., & Leighly, K. M. 1999, A&A, 350, L31
Grupe, D., et al. 1995, A&A, 299, L5
Gurzadian, V. G., & Ozernoi, L. M. 1981, A&A, 95, 39
Halpern, J., et al. 2004, ApJ, 604, 572
Heckman, T., Ptak, A., Hornschemeier, A., & Kauffmann, G. 2005, ApJ, 634, 161
Heng, K., & McCray, R. 2007, ApJ, 654, 923
Hills, J. G. 1975, Nature, 254, 295
Hjorth, J., et al. 2003, Nature, 423, 847
Hoffman, J. L., et al. 2008, ApJ, 688, 1186
Houck, J. R., et al. 2004, ApJS, 154, 18
Humphreys, R. M., & Davidson, K. 1994, PASP, 106, 1025
Hyland, A. R., & Allen, D. A. 1982, MNRAS, 199, 943
Immler, S. 2007, in AIP Conf. Proc. 937, Supernova 1987A: 20 Years After: Supernovae and Gamma-Ray Bursters, ed. S. Immler, K. Weiler, & R. McCray (Melville, NY: AIP), 246
Immler, S., Brown, P. J., Filippenko, A. V., & Pooley, D. 2007, ATeL, 1420, 1
Immler, S., & Pooley, D. 2007, ATeL, 1004, 1
Ivanov, P. B., & Chernyakova, M. A. 2006, A&A, 448, 843
Kato, M., & Hoshi, R. 1978, Prog. Theor. Phys., 60, 1692
Keenan, F. P., & Norrington, P. H. 1987, A&A, 181, 370
Khoklov, A., & Melia, F. 1996, ApJ, 457, L61
Klebesadel, R. W., Strong, I. B., & Olson, R. A. 1973, ApJ, 182, L85
Komossa, S. 2002, in Reviews in Modern Astronomy 15, ed. R. Schielicke (New York: Wiley-VCH), 27
Komossa, S., & Bade, N. 1999, A&A, 343, 775
Komossa, S., & Greiner, J. 1999, A&A, 349, L45
Komossa, S., & Merritt, D. 2008, ApJ, 683, L21
Komossa, S., & Schulz, H. 1997, A&A, 323, 31
Komossa, S., et al. 2004, ApJ, 603, L17
Komossa, S., et al. 2008, ApJ, 678, L13 (Paper I)
Kotak, R., et al. 2006, ApJ, 651, L117
Laguna, P., Miller, W. A., Zurek, W. H., & Davies, M. B. 1993, ApJ, 410, L83
Lamb, D. Q. 2000, ApJS, 127, 395
Lee, H. M., Kang, H., & Ryu, D. 1996, ApJ, 464, 131
Leonard, D. C., Filippenko, A., Barth, A., & Matheson, T. 2000, ApJ, 536, 239
Li, L.-X., Narayan, R., & Menou, K. 2002, ApJ, 576, 753
Lu, H., et al. 2006, AJ, 131, 790
Lu, Y., Huang, Y. F., & Zhang, S. N. 2008, ApJ, 684, 1330
Lucy, L. B., Danziger, I. J., Gouiffes, C., & Bouchet, P. 1989, in Structure and Dynamics of the Interstellar Medium, ed. G. Tenorio-Tagle et al. (Berlin: Springer), 164
Luminet, J.-P. 1985, Ann. Phys., 10, 101
Luminet, J.-P., & Marck, J.-A. 1985, MNRAS, 212, 57
Luminet, J.-P., & Pichon, B. 1989, A&A, 209, 103
Markwardt, C. B., et al. 2005, ApJ, 633, L77
Martin, D. C., et al. 2005, ApJ, 619, L1
Mazzali, P. A., et al. 2006, Nature, 442, 1018
Meikle, W. P. S., et al. 2006, ApJ, 649, 332
Merrill, K. M. 1980, IAU Circ., 3444, 3
Merritt, D. 2009, ApJ, 694, 959
Mohan, M., Hilbert, A., & Kingston, A. E. 1994, ApJ, 434, 389
Moseley, S. H., Dwek, E., Glaccum, W., Graham, J. R., Loewenstein, R. F., & Silverberg, R. F. 1989, Nature, 340, 697
Mullaney, J. R., & Ward, M. J. 2008, MNRAS, 385, 53
Nagao, T., Taniguchi, Y., & Murayama, T. 2000, AJ, 119, 2605
Netzer, H. 1974, MNRAS, 169, 579
Netzer, H., Mainieri, V., Rosati, P., & Trakhtenbrot, B. 2006, A&A, 453, 525
Netzer, H., et al. 2007, ApJ, 666, 806
Nussbaumer, H., & Storey, P. J. 1982, A&A, 113, 21

Oliva, E. 1997, ASP Conf. Ser. 113, Emission Lines in Active Galaxies: New Methods and Techniques; IAU Colloquium 159, ed. B. M. Peterson, F.-Z. Cheng, & A. S. Wilson (San Francisco, CA: ASP), 288
Oliva, E., Salvati, M., Moorwood, A. F. M., & Marconi, A. 1994, A&A, 288, 475
Osterbrock, D. E. 1969, Astrophys. Lett., 4, 57
Osterbrock, D. E. 1989, Astrophysics of Gaseous Nebulae (Mill Valley, CA: University Science Books)
Pastorello, A., et al. 2002, MNRAS, 333, 27
Pelan, J., & Berrington, K. A. 1995, A&AS, 110, 209
Penston, M. V., Fosbury, R. A. E., Boksenberg, A., Ward, M. J., & Wilson, A. S. 1984, MNRAS, 208, 347
Peterson, B. M., & Ferland, G. 1986, Nature, 324, 345
Piran, T. 2005, Rev. Mod. Phys., 76, 1143
Pozzo, M., et al. 2004, MNRAS, 352, 475
Puget, J.-L., & Leger, A. 1989, ARA&A, 27, 161
Quimby, R. M., et al. 2007, ApJ, 668, L99
Raymond, J. C. 1995, Ap&SS, 233, 231
Rees, M. J. 1988, Nature, 33, 523
Rees, M. J. 1990, Science, 247, 817
Renzini, A. 2001, in Black Holes in Binaries and Galactic Nuclei: Diagnostics, Demography, and Formation, ed. L. Kaper, E. P. J. van den Heuvel, & P. A. Woudt (Berlin: Springer), 161
Roche, P. F., Aitken, D. K., Smith, C. H., & James, S. D. 1989, Nature, 337, 533
Rosswog, S., Ramirez-Ruis, E., & Hix, R.W. 2008, arXiv:astro-ph/0811.2129
Schlegel, E. M. 1990, MNRAS, 244, 269
Schlegel, E. M. 1995, Rep. Prog. Phys., 58, 1375
Schlegel, E. M. 2006, in IAU Symp. 230, High-Energy Sources in Galaxies, ed. E. J. A. Meurs & G. Fabbiano (Cambridge: Cambridge Univ. Press), 252 (San Francisco, CA: ASP)
Schlegel, E. M., & Petre, A. 2006, ApJ, 646, 378
Schweitzer, M., et al. 2006, ApJ, 649, 79
Seyfert, C. K. 1943, ApJ, 97, 28
Shields, G. A., & Bonning, E. W. 2008, ApJ, 682, 756
Shull, M. J. 1980, ApJ, 237, 769
Skrutskie, M. F., et al. 2006, AJ, 131, 1163
Smartt, S. J., Eldrige, J. J., Crockett, R. M., & Maud, J. R. 2009, MNRAS, 395, 1409
Smith, N., et al. 2008a, ApJ, 686, 467
Smith, N., Foley, R. J., & Filippenko, A. V. 2008b, ApJ, 680, 568
Smith, N., et al. 2009, ApJ, in press (arXiv:0809.5079; S09)
Soderberg, A. M., et al. 2008, Nature, 453, 469
Stathakis, R. A., & Sadler, E. M. 1991, MNRAS, 250, 786
Stern, D., et al. 2004, ApJ, 612, 690
Storchi-Bergmann, T., et al. 1995, ApJ, 443, 617
Storchi-Bergmann, T., et al. 2003, ApJ, 598, 956
Sturm, E., et al. 2002, A&A, 393, 821
Sugerman, B. E. K., et al. 2006, Science, 313, 196
Sutherland, R. S., & Dopita, M. A. 1995, ApJ, 439, 381
Temple, R. F., Raychaudhury, S., & Stevens, I. R. 2005, MNRAS, 362, 581
Terlevich, R., & Melnick, J. 1988, Nature, 333, 239
Tommasin, S., et al. 2008, ApJ, 676, 836
Turatto, M., Capellaro, E., Danziger, I. J., Bentti, S., Gouiffes, C., & Della Valle, M. 1993, MNRAS, 262, 128
Turatto, M., et al. 2000, ApJ, 534, L57
van Dyk, S. D., Weiler, K. W., Sramek, R. A., & Panagia, N. 1993, ApJ, 419, L69
Vaughan, S., Edelson, R., & Warwick, R. S. 2004, MNRAS, 349, 1
Veilleux, S. 1988, AJ, 95, 1695
Viegas-Aldrovandi, S. M., & Contini, M. 1989, A&A, 215, 253
Voges, W., et al. 1999, A&A, 349, 389
Wegner, G., & Swanson, S. R. 1996, MNRAS, 278, 22
Weiler, K. W., Panagia, N., & Sramek, R. A. 1990, ApJ, 364, 611
Wheeler, J. C., Mazurek, T. J., & Sivaramakrishnan, A. 1980, ApJ, 237, 781
Willner, S. P., et al. 1984, PASP, 96, 143
Wooden, D. H., et al. 1993, ApJS, 88, 477
Woosley, S. E., & Bloom, J. S. 2006, ARA&A, 44, 507
Wright, E. L. 2006, PASP, 118, 1711
Young, P. J., Shields, G. A., & Wheeler, J. C. 1977, ApJ, 212, 367
Zhou, H.-Y., et al. 2006, ApJS, 166, 128